

THE $Z \sim 6$ LUMINOSITY FUNCTION FAINTER THAN -15 MAG FROM THE *HUBBLE* FRONTIER FIELDS: THE IMPACT OF MAGNIFICATION UNCERTAINTIES

R.J. BOUWENS¹, P.A. OESCH^{2,3}, G.D. ILLINGWORTH⁴, R.S. ELLIS^{5,6}, M. STEFANON¹

Draft version November 12, 2018

ABSTRACT

The *Hubble* Frontier Fields (HFF) program has substantial potential for constraining both the properties and prevalence of faint galaxies in the early universe. Yet the accuracy of results derived in high magnification regions using lensing clusters is limited due to systematics. We present a new forward-modeling formalism to incorporate the impact of magnification uncertainties into luminosity function results, by exploiting the availability of many independent magnification models for the same clusters. One public magnification model is treated as the truth and used to construct a mock set of lensed high-redshift galaxies, which can then be analyzed using another magnification model (typically a median model) to construct a luminosity function. Using the most comprehensive and faintest selection of lensed $z \sim 6$ galaxies to date (drawn from the first 4 HFF clusters), we then derive direct constraints on the shape of the UV LF to -13.5 mag and with much greater uncertainties to -12.5 mag. Our simulations reveal that for highly-magnified sources ($\gtrsim 30\times$) the systematic uncertainties become very large, reaching *several orders of magnitude* at 95% confidence at ~ -12 mag. The volume densities we derive for faint (> -17 mag) sources are $\sim 3\text{--}4\times$ lower than one recent report, with a faint-end slope -1.92 ± 0.04 (3.5σ shallower). Introducing a new curvature parameter to model the faint end of the LF, we demonstrate that current observations permit (within the 68% confidence intervals) a turn-over in the $z \sim 6$ UV LF as bright as -15.3 and -14.2 mag, respectively, if differences between the full and parameterized set of lensing models in the HFF effort are representative. We discuss the implications of such a turn over in the context of recent theoretical predictions.

1. INTRODUCTION

One of the most important open question in extragalactic studies regards cosmic reionization and clarifying which sources drive this important phase transition in the early universe. While much evidence suggests that the process might be driven by galaxies (e.g., Robertson et al. 2013, 2015; Mitra et al. 2015; Bouwens et al. 2015), others have suggested that quasars could provide the dominant contribution (Giallongo et al. 2015; Madau & Haardt 2015; Mitra et al. 2016).

The important issues appear to be whether large numbers of faint quasars exist at high redshift (e.g., Willott et al. 2010; McGreer et al. 2013), whether faint galaxies show an appreciable ($>5\%$) escape fraction (e.g., Siana et al. 2010, 2015; Vanzella et al. 2012, 2016; Nestor et al. 2013), and what the total emissivity is in the rest-frame UV in faint galaxies beyond the limits of current surveys in the *Hubble* Ultra Deep Field (HUDF: Beckwith et al. 2006; Ellis et al. 2013; Illingworth et al. 2013). Important issues for the latter question are the precise values of the faint-end slopes and the faint-end cut-off to the UV luminosity function. Depending on the value of the faint-end slope and the luminosity where a cut-off in the

LF occurs (Kuhlen & Faucher-Giguère 2012; Bouwens et al. 2012; Robertson et al. 2013; Bouwens 2016), the total emissivity from galaxies in the UV can vary by factors of $\sim 2\text{--}10$.

One potentially promising way to constrain the total luminosity density in the rest-frame UV is by taking advantage of the impact of gravitational lensing by galaxy clusters for magnifying individual sources. This can bring extremely faint galaxies into view such that they can be detected with current telescopes (e.g., Bradac et al. 2009; Maizy et al. 2010; Coe et al. 2015). There has been a significant investment in this approach by *HST* in the form of the *Hubble* Frontier Fields program (Coe et al. 2015; Lotz et al. 2016), which is investing 840 orbits into reaching ~ 29 -mag in 7 optical+near-IR bands, as well as two UVIS channels in a supporting effort (Alavi et al. 2016; Siana 2013, 2015).

Already, analyses of sources behind the HFF clusters have resulted in the identification of $z \sim 6\text{--}8$ sources first to -15 mag (Atek et al. 2015a,b) and later to ~ -13 mag (Kawamata et al. 2016; Castellano et al. 2016a,b; Livermore et al. 2016 [hereinafter, L16]). At $z \sim 2\text{--}3$, it has been similarly possible (Alavi et al. 2014, 2016) to probe to ~ -13 mag taking advantage of very deep WFC3/UVIS observations over Abell 1689 and various clusters in the HFF program. Based on these deep searches, the volume density of galaxies at > -16 mag have been estimated, with quoted faint-end slopes for $z \sim 2\text{--}3$ LFs that range from -1.6 to -1.9 (Alavi et al. 2014, 2016) and from -1.9 to -2.1 for $z \sim 6\text{--}8$ LFs (Atek et al. 2015a,b; Ishigaki et al. 2015; Laporte et al. 2016; Castellano et al. 2016b; L16), respectively.

In spite of the great potential that lensing clusters have for probing the faint end of the UV LF, successfully mak-

¹ Leiden Observatory, Leiden University, NL-2300 RA Leiden, Netherlands

² Department of Astronomy, Yale University, New Haven, CT 06520

³ Observatoire de Genève, 1290 Versoix, Switzerland

⁴ UCO/Lick Observatory, University of California, Santa Cruz, CA 95064

⁵ European Southern Observatory (ESO), Karl-Schwarzschild-Strasse 2, 85748 Garching, Germany

⁶ Department of Physics and Astronomy, University College London, Gower Street, London, WC1E 6BT, UK

ing use of data over these clusters to perform this task in an accurate manner is not trivial. The entire enterprise is fraught with sources of systematic error. One of these sources of systematic error concerns the assumed size distribution of extremely faint galaxies (Bouwens et al. 2016; Grazian et al. 2011; Oesch et al. 2015). Small differences in the assumed half-light radii have the potential to change the inferred faint-end slopes by large factors, i.e., $\Delta\alpha \gtrsim 0.3$ depending on whether the mean size of extremely faint galaxies is 120 mas, 30 mas, or 7.5 mas (e.g., see Figure 2 from Bouwens et al. 2016). Fortunately, we found that most of the extremely faint sources seem consistent with being almost unresolved, i.e., with intrinsic sizes of <10 -30 mas (Bouwens et al. 2016; see also Kawamata et al. 2014; Laporte et al. 2016), making this issue much more manageable in terms of its impact; but it still remains an uncertainty. A second source of systematic error arises from errors in the magnification maps, since this can have a profound impact on the LFs derived. Finally, there are issues related to subtraction of the foreground cluster light, contamination from individual sources in the clusters (e.g., globular clusters), and from other less important systematic effects that affect determinations of the volume densities in the field vs. the cluster.⁷

Even without such considerations, it is easy to see that systematics could be a concern for LF studies from lensing clusters, simply by comparing several recent LF results from clusters with similar results based on deep field studies using the HUDF. To give one recent example, Alavi et al. (2016) reported a faint-end slope α of -1.94 ± 0.06 for the *UV* LF at $z \sim 3$ based on an analysis of sources behind 3 lensing clusters, while Parsa et al. (2016) reported a faint-end slope of -1.31 ± 0.04 based on a deep $z \sim 3$ search over the HUDF. These results differ at a significance level of $\sim 9\sigma$ taking at face value the quoted statistical errors. This is but one example of the large differences frequently present between LF results derived from deep field studies and those derived on the basis of lensing clusters (see Figure 1 for several other examples).

In addition to the clear scientific importance of the faint-end slope α for computing the total ionizing emissivity from faint galaxies, the observations also allow us to test for a possible flattening or turn-over of the *UV* LF at low luminosities. Many cosmological hydrodynamic simulations of galaxy formation predict a flattening in the *UV* LF at ~ -13 or ~ -15 due to less efficient atomic and molecular hydrogen cooling, respectively (Muñoz & Loeb 2011; Krumholz & Dekel 2012; Kuhlen et al. 2013; Jaacks et al. 2013; Wise et al. 2014; Liu et al. 2016a; Gnedin 2016; Finlator et al. 2016), while other simulations predict a flattening in the range ~ -16 to ~ -13 mag due to the impact of radiative feedback (O’Shea et al. 2015; Ocvirk et al. 2016). Meanwhile, by combining abundance matching and detailed studies of color-magnitude diagram of low-luminosity dwarfs in

⁷ For example, the HFF program does not feature deep observations in the z_{850} -band, which is useful for discriminating between $z \sim 6$ and $z \sim 7$ galaxies, while the HUDF and CANDELS (Grogin et al. 2011; Koekemoer et al. 2011) programs do feature deep integrations in this filter. The availability or not of deep observations in the z_{850} band could impact the $z \sim 6$ and $z \sim 7$ samples and LF results derived from these data sets in different ways.

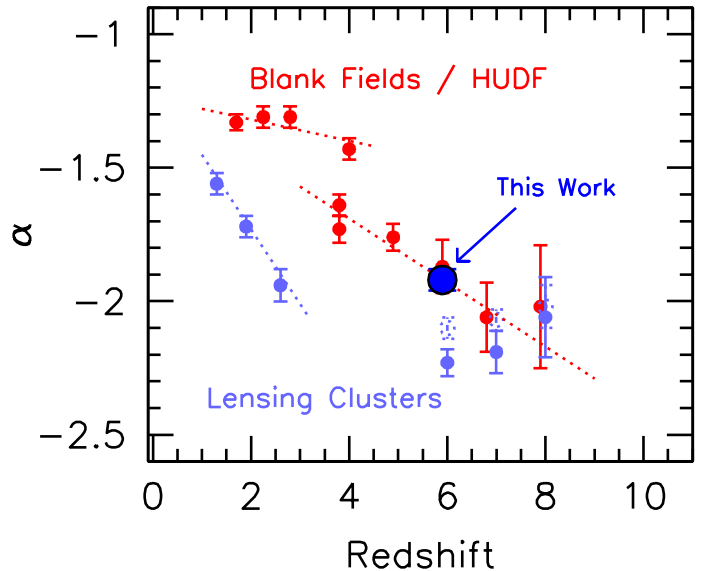


FIG. 1.— Some recent measurements of the faint-end slope α vs. redshift from the literature using deep fields (red solid circles) and using lensing clusters (light blue solid circles). The field LF results are from Parsa et al. (2016) at $z \leq 4$, Bouwens et al. (2007) at $z \sim 4$, and Bouwens et al. (2015) at $z \geq 4$. The $z \leq 3$ cluster LF results are from Alavi et al. (2016). The $z = 6$ -8 cluster LF results shown are based on a fit to the L16 cluster stepwise LFs anchored to one point (-20 mag) at the bright end of the field LF (see Appendix D). This ensures that the presented faint-end slope α results from L16 are almost entirely independent of field constraints; the nominal faint-end slope results from L16 (including constraints from the field) are shown with the dotted open circles. The large solid dark blue shows the faint-end slope α we estimate from our $z \sim 6$ HFF cluster sample in §4. As field and lensed LFs potentially probe different luminosity regimes in the *UV* LF (bright and fainter, respectively), it is possible there would be slight differences in the derived slopes; however, the differences run in the opposite direction normally predicted in simulations (e.g., see right panel in Figure 1 from Gnedin 2016). Given that the differences between the derived α 's are often much larger than the plotted statistical error bars, systematic errors must clearly contribute substantially to some of the determinations plotted here.

the local universe, evidence for a low-mass turn-over in the luminosity function has been reported at -13 mag (Boylan-Kolchin et al. 2015; see also Boylan-Kolchin et al. 2014). Current observations likely provide us with some constraints in this regime. However, given the significant systematics that appear to be present in current determinations of the faint-end slope α from lensing clusters (vs. field results), it is not at all clear that current constraints on the form of the *UV* LF at > -15 mag are reliable, particularly at $z > 4$.

In the present paper, we take the next step in our examination of the impact of systematic errors on derived LF results from lensing clusters, after our previous paper on this subject, i.e., Bouwens et al. (2016), where the emphasis was on the uncertain sizes of faint sources. Here the focus will be more on the uncertainties in LF results that arise from errors in the gravitational lensing models. As we will demonstrate explicitly, the recovered LF from a straightforward analysis tends to migrate towards a faint-end slope of ~ -2 (or slightly steeper), if uncertainties in the magnification factor are large. The impact of these uncertainties is to wash out features in the LF, particularly at low luminosities. Given that magnification factors μ necessarily become uncertain when these

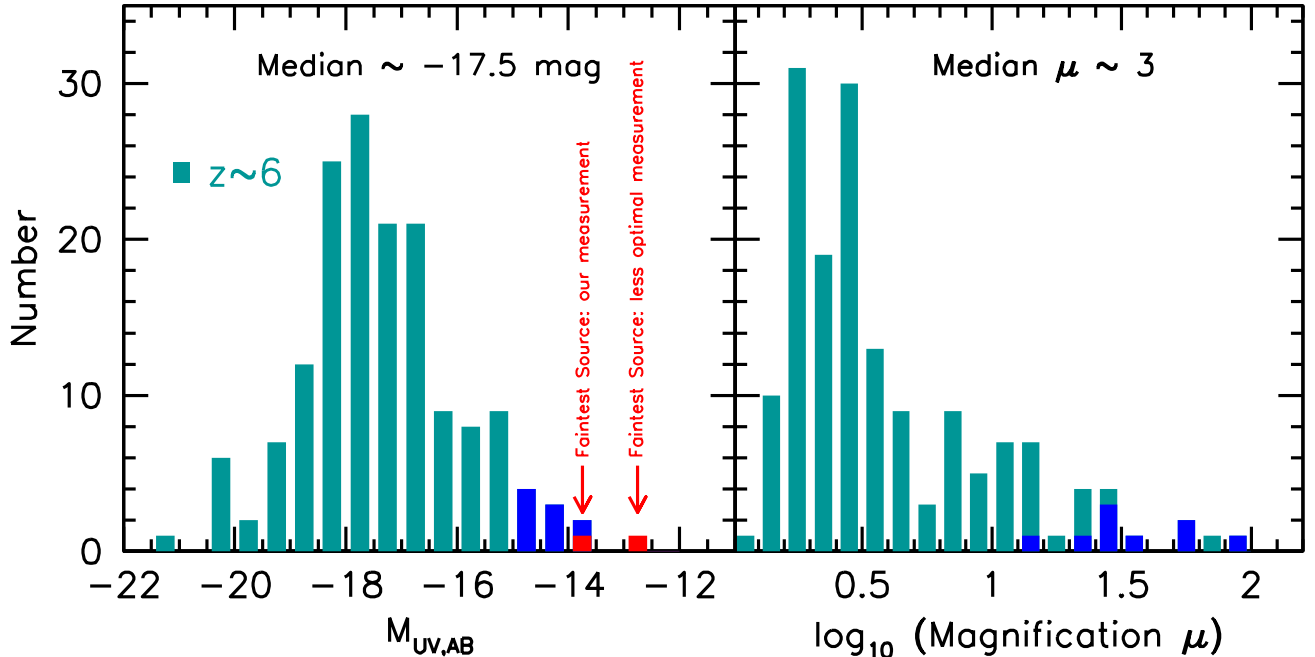


FIG. 2.— Number of galaxies found in our conservative selection of $z \sim 6$ galaxies behind the first four HFF clusters vs. their inferred M_{UV} luminosity (*left panel*) and magnification factor (*right panel*). We take the magnification factor to be the median of those derived from the four parametric models (GLAFIC, CATS, Sharon/Johnson, and Zitrin-NFW), enforcing a maximum value of 100 (due to the much weaker predictive power for the models at such high magnification factors: see Figure 3). The nine sources with the faintest intrinsic luminosities are shown in blue in each panel. The faintest source in our probe is sensitive to how total magnitude measurements are made. The two red squares show the luminosity of our faintest source, as we measure it with our total flux approach (*left red square*) and also (*right red square*) consistent with the way that L16 measure luminosities for many of the sources in their $z \sim 6-8$ samples (see §2 and §6.1.2). The luminosity shifts ~ 0.7 mag faintward for these sources in the latter approach.

factors are high, i.e., $\mu > 10$ and especially $\mu > 50$, accurately constraining the shape of the LF at extremely low luminosities and also detecting a turn-over or flattening is very challenging.

The purpose of this paper is to look at the constraints we can set on the faint end of the $z \sim 6$ UV LF with a thorough assessment of the possible systematic errors. In doing so, we will look for possible evidence for a turn-over in the LF at very low luminosities and if not present, what constraints can be placed on the luminosity of a turn-over. Evidence for a turn-over will be evaluated through the introduction of a *curvature parameter* which we constrain through extensive Markov-Chain Monte-Carlo (MCMC) trials. The confidence intervals we obtain on the shape of the UV LF at faint magnitudes will provide theorists with some important constraints for comparison with models and cosmological hydrodynamic simulations. Most importantly, these results provide balance to some discussion in the literature arguably making premature claims for the LF rising steeply to very low luminosities. To keep the focus of this paper on our new techniques, we restrict our analysis to just the $z \sim 6$ LF from the first four HFF clusters.

The plan for this paper is as follows. §2 summarizes the data sets we use to select our $z \sim 6$ sample and derive constraints on the $z \sim 6$ LF. §3 provides some useful context for the issue of errors in the magnification models and shows the general impact it would have on LF results. §4 and §5 present new LF results at $z \sim 6$ using our new forward-modeling methodology. §6 compares our new results with previous reported LF results,

as well as results from various theoretical models. Finally, in §7, we summarize and conclude. We refer to the HST F814W, F850LP, F105W, F125W, F140W, and F160W bands as I_{814} , z_{850} , Y_{105} , J_{125} , JH_{140} , and H_{160} , respectively, for simplicity. Through this paper, a standard “concordance” cosmology with $H_0 = 70 \text{ km s}^{-1} \text{ Mpc}^{-1}$, $\Omega_m = 0.3$ and $\Omega_\Lambda = 0.7$ is assumed. This is in good agreement with recent cosmological constraints (Planck Collaboration et al. 2015). Magnitudes are in the AB system (Oke & Gunn 1983).

2. DATA SETS AND $Z \sim 6$ SAMPLE

In our selection of $z \sim 6$ galaxies, we make use of the v1.0 reductions of the deep *HST* optical and near-IR *HST* observations available over the first four clusters in the HFF program: Abell 2744, MACS0416, MACS0717, and MACS1149 (A. Koekemoer et al. 2016, in prep). The optical observations include ~ 18 , ~ 10 , and ~ 42 orbits of ACS observations in the F435W, F606W, and F814W bands from $0.4\mu\text{m}$ to $0.9\mu\text{m}$. Near-IR observations over these fields total 34, 12, 10, and 24 orbits in the F105W, F125W, F140W, and F160W, reaching to roughly a 5σ limiting magnitude of 28.8 to 29.0 mag.

Subtraction of foreground light from cluster galaxies and cluster galaxies was performed using galfit (Peng et al. 2002) and the median-filtering algorithm of SExtractor (Bertin & Arnouts 1996) run at two different grid scales. There are many similarities of our procedure to that from Merlin et al. (2016). The only areas clearly inaccessible to us in our searches for faint $z \sim 6$ galaxies occur directly under the cores of bright stars or galaxies

TABLE 1
MAGNIFICATION MODELS USED HERE^a

Model Name	Mass-Traces-Light	Dark-Matter	Code	Parametric ^b	Resolution (")	References
“Parametric” Models ^b						
GLAFIC	Y	Y	GLAFIC	Y	0.03"	Oguri (2010); Ishigaki et al. 2015; Kawamata et al. (2016)
CATS	Y	Y	LENSTOOL	Y	0.1"	Jullo & Kneib (2009); Richard et al. (2014); Jauzac et al. (2015a,b)
Sharon/Johnson	Y	Y	LENSTOOL	Y	0.06"	Johnson et al. (2014)
Zitrin-NFW	Y	Y	Zitrin	Y	0.06"	Zitrin et al. (2013, 2015)
“Non-Parametric” Models						
GRALE	N	Y	GRALE	N	0.22"	Liesenborgs et al. (2006); Sebesta et al. (2016)
Bradac	N	Y	Bradac	N	0.2"	Bradac (2009)
Zitrin-LTM	Y	N	Zitrin	N	0.06"	Zitrin et al. (2012, 2015).

^a This includes all publicly available lensing models which have high-resolution mass maps and are generally available for the first four HFF clusters. Our analyses therefore do not include the public HFF models of Diego et al. (2015) and Merten et al. (2015).

^b Parametric models assume that mass in the cluster is in the form of one or more dark matter components with an ellipsoidal Navarro-Frenk-White (NFW: Navarro et al. 1997) form and to include a contribution from galaxies following specific mass-to-light scalings. Two well-known parametric modeling codes are LENSTOOL (Jullo & Kneib 2009) and GLAFIC (Oguri 2010).

in the cluster. Our procedure performs at least as well as any other procedure currently in use (Merlin et al. 2016; L16). While the approach used by L16 appears to be a good one, there is no evidence it is better than the procedures presented by Merlin et al. (2016) or the approach we have developed.

A complete description of both our photometric procedure and selection criteria for identifying $z \sim 6$ galaxies is provided in R.J. Bouwens et al. (2016, in prep). It remains similar to that done in many of our previous papers (e.g., Bouwens et al. 2015). We briefly summarize our criteria here for selecting a robust and large sample of $z \sim 6$ galaxies. We select all sources that satisfy the following I_{814} -dropout color criteria

$$(I_{814} - Y_{105} > 0.6) \wedge (Y_{105} - H_{160} < 0.45) \wedge (I_{814} - Y_{105} > 0.6(Y_{105} - H_{160})) \wedge (Y_{105} - H_{160} < 0.52 + 0.75(J_{125} - H_{160}))$$

and which are detected at $>6.5\sigma$ adding in quadrature the S/N of sources in the Y_{105} , J_{125} , JH_{140} , and H_{160} band images measured in a $0.35''$ -diameter aperture. The above color selection criterion also explicitly excludes the inclusion of $z \sim 8$ Y_{105} -dropout galaxies. As the above criteria identify sources at both $z \sim 6$ and $z \sim 7$, we compute the redshift likelihood function $P(z)$ for each source and only include those sources where the best-fit photometric redshift is less than 6.3. Sources are further required to have a cumulative probability $<35\%$ at $z < 4$ to keep contamination to a minimum in our high-redshift samples.

Our sample of 160 $z \sim 6$ candidate galaxies is the largest compilation reported to date. Each of the HFF clusters we examine in this study have at least seven independent lensing models available, with both convergence κ and shear γ maps (Table 1). We estimate the magnification of sources based on publicly-available models by first multiplying the κ and γ maps of each cluster by D_{ls}/D_s and then computing the magnification μ as follows:

$$\mu = \frac{1}{|(1 - \kappa)^2 - \gamma^2|} \quad (1)$$

For our magnification estimates for individual sources,

we take the median of the model magnifications from the CATS (Jullo & Kneib 2009; Richard et al. 2014; Jauzac et al. 2015a,b), GLAFIC (Oguri 2010; Ishigaki et al. 2015; Kawamata et al. 2016), Sharon/Johnson (Johnson et al. 2014), and Zitrin parametric NFW models (Zitrin-NFW: Zitrin et al. 2013, 2015). The parametric models generally provided the best estimates of the magnification for individual sources in the HFF comparison project (Meneghetti et al. 2016), but we emphasize that many non-parametric magnification models also performed very well.

We present in Figure 2 the distribution of absolute magnitudes and magnification factors we estimate for sources in our $z \sim 6$ sample. We set an arbitrary maximum magnification factor of 100, given the lack of predictive power for magnification maps at such high values (see §3.1). This constraint affects very few sources. Our selection includes sources ranging from -22 mag to -13.5 and with magnification factors ranging from 1.2 to 50, with the bulk of the sources having absolute magnitudes of -18 and magnification factors of ~ 2 .

We should emphasize that the inferred luminosities and total magnitudes we report for sources are intended to provide a rather complete accounting for light in individual sources. They are based on scaled-aperture photometry following the Kron (1980) method, with a correction for flux on the wings of the PSF (e.g., see Bouwens et al. 2015). However, in comparing our total magnitude measurements with the magnitude measurements from other groups (e.g., L16: see §6.1.2), we have found some sources being reported to have apparent magnitude measurements fainter by ~ 0.7 - 1.0 mag than what we measure for the same sources (including the very faint -12.4 source reported by L16 that anchors their LF at the faint end: see §6.1.2 and §6.2).

If we quote the luminosities of sources in our study using a similar procedure as to what L16 appear to use – where individual sources are often ~ 0.7 - 1.0 mag fainter than we find – our probe would extend to -12.6 mag (indicated in Figure 2 with the red bin), essentially identical to that claimed by L16 (see also Castellano et al. 2016 and Kawamata et al. 2016). We emphasize, however, that the low luminosities claimed by measuring magni-

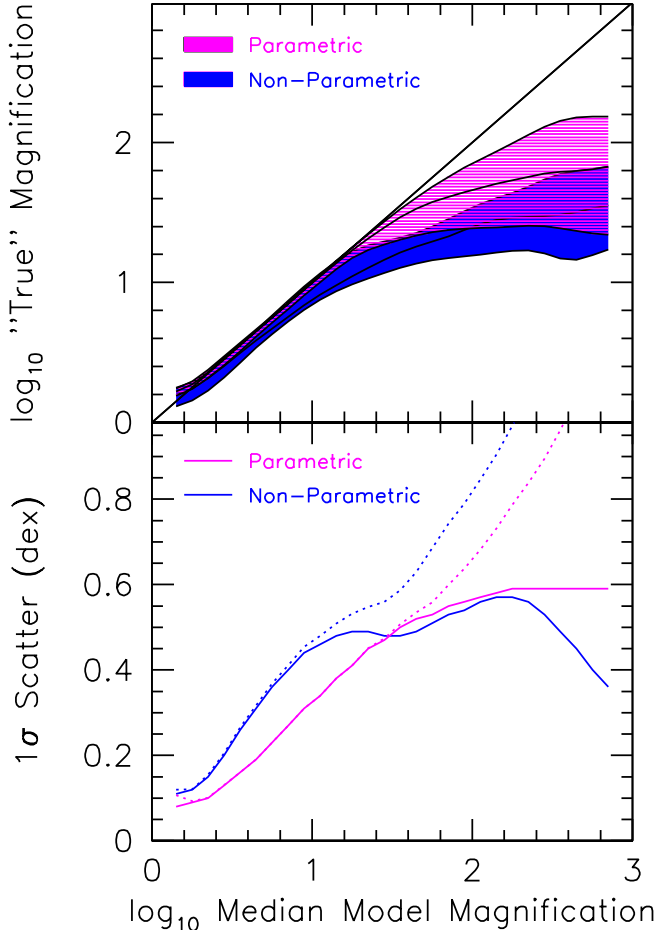


FIG. 3.— An evaluation of the predictive power of the lensing models. (*upper*) Illustration of how well the magnification factors (*magenta-shaded region plotted on the vertical axis*) in a given parametric model (i.e., GLAFIC, CATS, Sharon/Johnson, Zitrin-NFW) can be predicted using the median magnification factors (*plotted on the horizontal axis*) from the other parametric lensing models. The blue-shaded region shows how well the magnification factors in the non-parametric models (GRALE, Bradac, and Zitrin-LTM) can be predicted by the other lensing models. Results on the vertical axis are presented in terms of the median magnification factors recovered from the other models for a given cluster. The upper envelope of the shaded region shows the results for the cluster with the highest recovered median magnification factor based on the other models, while the lower envelope shows results for the cluster with lowest recovered median magnification factor. The black line shown inside the center of each of the shaded regions is the geometric mean of the recovered medians for the first four HFF clusters. (*lower*) 1σ scatter in the magnification factors for a given parametric model predicted using a median of the other models (*magenta solid line*). The blue solid line gives the results for the non-parametric models. The dotted lines are the same as the solid lines but also add in quadrature the logarithmic differences between the actual magnification factors in a model and that predicted from a median of the other models. From this figure, it is clear that the median magnification model has largely lost its predictive power by magnification factors of ~ 10 and ~ 30 assuming that the available non-parametric and parametric models, respectively, are representative of reality.

tudes in this way exaggerate how faint the HFF program probes. We discuss this further in §6.1.2 and §6.2. We prefer our photometric scheme for accounting for the total light in faint sources.

3. IMPACT OF MAGNIFICATION ERRORS ON THE DERIVED LFS

An important aspect of the present efforts to provide constraints on the $z \sim 6$ LF will be our explicit efforts to include a full accounting of the uncertainties present in the magnification models we utilize. We begin by looking first at the general size of errors in the magnification models and second at how the errors would impact LFs derived from lensing clusters.

3.1. Predictive Value of the Public Magnification Models

In making use of various gravitational lensing models to derive constraints on the prevalence of extremely faint galaxies at high redshift, it is important to obtain an estimate of how predictive the lensing models are for the true magnification factors.

One way of addressing this issue is the fully end-to-end approach pursued by Meneghetti et al. (2016) and involves constructing highly-realistic mock data sets, analyzing the mock data sets using exactly the same approach as are used on the real observations, and then quantifying the performance of the different methods by comparing with the actual magnification maps. While each of the methods did fairly well in reproducing the magnification maps to magnification factors of ~ 10 , the best performing methods for reconstructing the magnification maps of clusters were the parametric models, with perhaps the best reconstructions achieved by the GLAFIC models, the Sharon/Johnson models, and the CATS models.

An alternate way of addressing this issue is by comparing the public lensing models against each other. Here we pursue such an approach. We treat one of the models as the truth and then to quantify the effectiveness of the other magnification models taken as a set for predicting that model's magnification map. We consider both the case that the true mass profile of the HFF clusters is considered (1) to lie among parametric class of models built on NFW-type mass profiles and (2) to lie among the non-parametric class of models which allow for more freedom in the modeling process. We take the former models to include the GLAFIC, CATS, Sharon/Johnson, and Zitrin-NFW models, and the latter to include the Bradac [2009], GRALE [Liesenborgs et al. 2006; Sebesta et al. 2016], and Zitrin-LTM [Zitrin et al. 2012, 2015].⁸ A brief description of the general properties of the public lensing models can be found in Table 1. In performing this test, we assume that the median of the magnification models provides our best means for predicting magnifications in the model we are treating as the truth. The truth model is always excluded when constructing the median magnification map for this test.

The results of this exercise are presented in the upper panel of Figure 3 for both the parametric and

⁸ Zitrin-LTM does not technically qualify as parametric or non-parametric, since the mass profile is governed by the distribution of light in a cluster. However, since the model shows a greater dispersion relative to the parametric models, we include it in the non-parametric group.

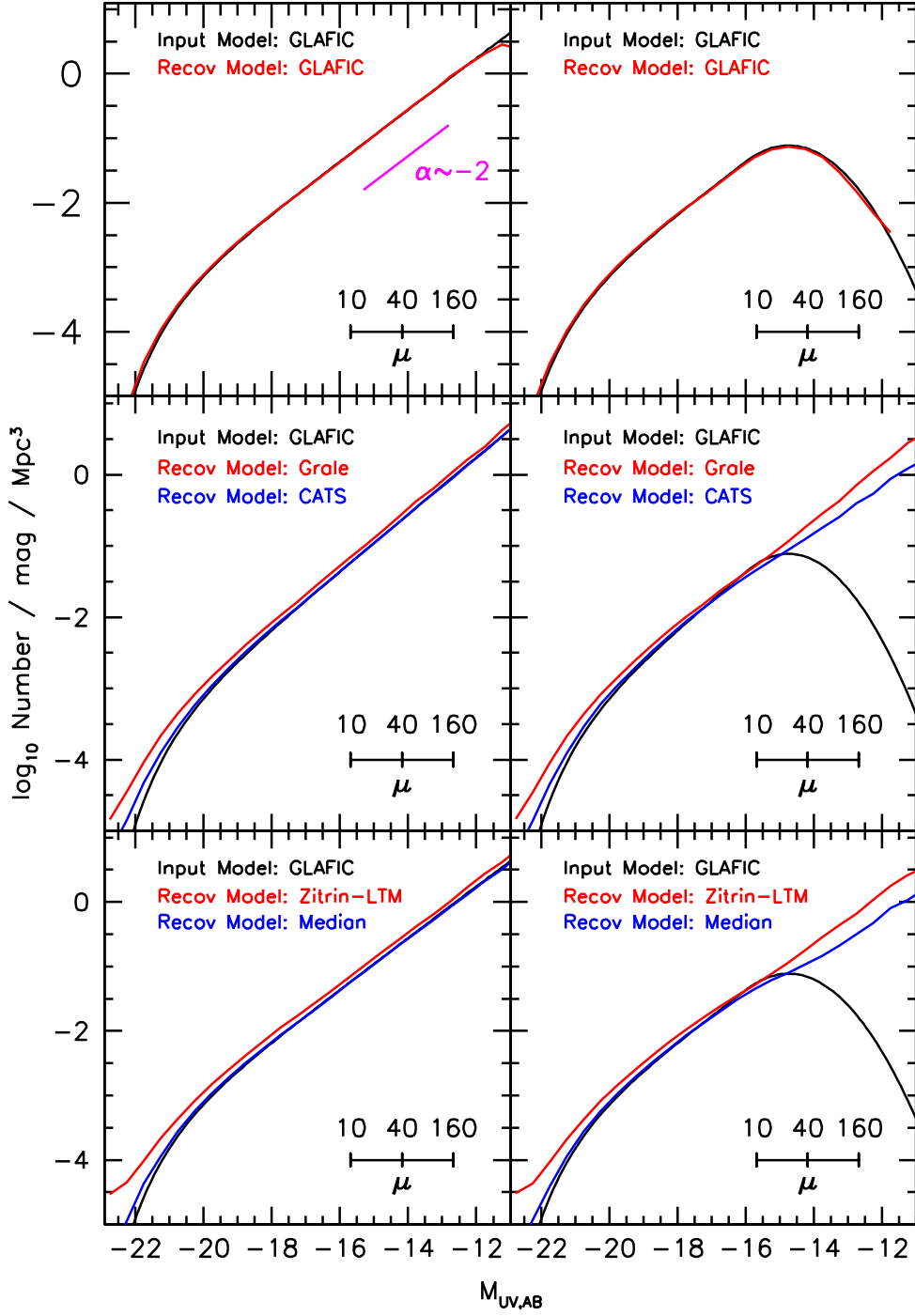


FIG. 4.— Comparison of the input LFs (black lines) into our forward-modeling simulations and the recovered LFs when using the same magnification models (top panels) and when using four different magnification models, including GRALE (red lines: middle panels), CATS (blue lines: middle panels), Zitrin-LTM (red lines: lower panels), and the median parametric model (blue lines: lower panels). A ticked horizontal bar is added to the panels to indicate the approximate luminosities probed by sources of a given magnification factor near the faint end of the HFF data set, i.e., 28.5 mag. Two input LFs are considered: one where the LF exhibits a faint-end slope of -2 with no turn-over at low luminosities (left panels) and a second also exhibiting a faint-end slope of -2 but with a turn-over at -15 mag (right panels). In the first case, the recovered LFs show a faint-end slope α of -2 to very low luminosities, in agreement with the input LF. However, for the second case, the recovered LFs again show a faint-end slope α of -2 to very low luminosities, in significant contrast to the input LF. As a result, interpreting the LF results from lensing clusters can potentially be tricky, as the detection of a turn-over in the LF at > -15 mag is very challenging (see §3.2). This is due to the weaker predictive power of the magnification models at high magnification factors $\mu > 10$ and especially $\mu > 30$ (Figure 3). See also Figures 14 and 15 from Appendices B and C.

non-parametric model cases. The geometric mean of the predictive power for each of the parametric (GLAFIC, CATS, Sharon/Johnson, Zitrin-NFW) and non-parametric (GRALE, Bradac, Zitrin-LTM) models is presented as an assessment of the predictive power of each approach for similar classes of models. The upper and lower bounds of the shaded regions give the predictive power for models corresponding to best and worst performing cluster, while the solid line in the center of the shaded region gives the median performance. The lower panel of Figure 3 shows the position-to-position scatter around the median magnification in the model treated as the truth. From this exercise, it is clear that the magnification maps have excellent predictive power to magnification factors of ~ 10 in all cases and perhaps to even higher magnification factors assuming that the magnification profiles of HFF clusters are as well behaved as in the parametric models. The scatter, however, is already very large at magnification factors of 10. We will extend this exercise in a future work (R.J. Bouwens et al. 2016, in prep).

The exercise we perform in this section shows similarities in philosophy to the analyses that Prieue et al. (2016) pursue, in comparing magnification models over the HFF clusters with each other to determine the probable errors in the individual magnification maps. One prominent conclusion from that study was that differences between the magnification maps was almost always larger than the estimated errors in the magnification for a given map, pointing to large systematics in the construction of the individual maps. This provides some motivation for the tests we perform here and in future sections in this paper, and confirmation of the importance of this study. Other powerful tests of the predictive power of the magnification maps, and the challenges, were provided by observations of SNe Ia (Rodney et al. 2015).

3.2. Impact of Magnification Errors on the Recovered LFs

The purpose of this subsection is illustrate the impact of magnification errors on the derived LFs from the HFF clusters. Two different example LFs are considered for this exercise: (1) one with a faint-end slope of -2 and a turn-over at -15 and (2) another with a fixed faint-end slope α of -2 and no turn-over.

How well can we recover these LFs given uncertainties in the magnification maps? We can evaluate this by generating a mock catalog of sources for each of the first four clusters from the HFF program using one set of magnification models (“input” models) and then attempting to recover the LF using another set of magnification models (“recovery” models). In computing the impact of lensing, the redshifts are fixed to $z = 6$ for all sources. The input magnification models are taken to be the GLAFIC models for this exercise. These catalogs include positions and magnitudes for all the individual sources in each cluster. The selection efficiencies of sources are accounted for when creating the mock catalogs, as estimated in Appendix A. In performing this exercise, we ignore errors in our estimates of the selection efficiencies and small number statistics at the faint end of the LF.

One can try to recover the input LFs from these mock

catalogs, using various magnification models. Sources are binned according to luminosity using the “recovery” magnification model. The selection volumes available in each luminosity bin are also estimated as described in Appendix A using this “recovery” magnification model. To demonstrate the overall self-consistency in our approach, we show the recovered LFs using the same magnification model as we used to construct the input catalogs in the top two panels in Figure 4.

What is the impact if different lensing models are used to recover the LF than those used to construct the mock catalogs? The lowest two rows of panels in Figure 4 show the results using the latest magnification models by GRALE, CATS, Zitrin-LTM, and the median of the CATS, Sharon/Johnson, and Zitrin-NFW models where available.

These simulation results demonstrate that the recovery process appears to work very well for input LFs with faint-end slopes of -2 (*left panels* in Figure 4) independent of the magnification model, with all recovered LFs showing a very similar form to the input LFs.

Very different results are, however, obtained in our attempts to recover input LFs with a turn-over at -15 mag (*right panels* in Figure 4) using magnification models that are different from the input model. For all four magnification models we consider, the recovered LFs look very similar to the LF example we just considered. All recovered LFs show a steep faint-end slope to -11 mag. What is striking is that they do not reproduce the turn-over present in the input model at -15 mag. There are some differences in the recovered LFs depending on how similar the input magnification model is to the recovery model, with effective faint-end slopes of -2 , -1.8 , and -1.7 achieved with the GRALE and Zitrin-LTM models, the CATS models, and the median parametric models, respectively. The GLAFIC magnification model is not used when constructing the median parametric magnification model.

Both examples demonstrate that the faint-end slope for the recovered LFs tend to gravitate towards a value of -2 . The faint-end slope of -2 results from magnification errors (that become large for $\mu > 20$) trading off with selection volume errors so as to scatter sources towards (1) higher luminosities and lower volume densities or (2) lower luminosities and higher volume densities. In either case, the scatter runs approximately parallel to a faint-end slope α of -2 (or slightly steeper depending on the intrinsic sizes of sources: see Appendix B).

Two other examples of the impact of large magnification errors on LF results are presented in Figures 14 and 15 in Appendices B and C, utilizing an input LF with a faint-end slope of -1.3 . For each of these examples, the recovered LF closely matches the input LF; dramatically, however, faintward of -15 mag (and even -16 mag for some models), the recovered LFs steepen and asymptote again towards a faint-end slope of ~ -2 (or steeper if sources are resolved), even if the actual slope of the LF is much shallower (or the LF turns over!).

Each of these examples demonstrate that, regardless of the input LF, a faint-end slope α of ~ -2 will be recovered whenever the magnification uncertainties are large. One cannot, therefore, use the consistent recovery of a steep faint-end slope based on a large suite of lensing models to argue that the actual LF maintains a steep

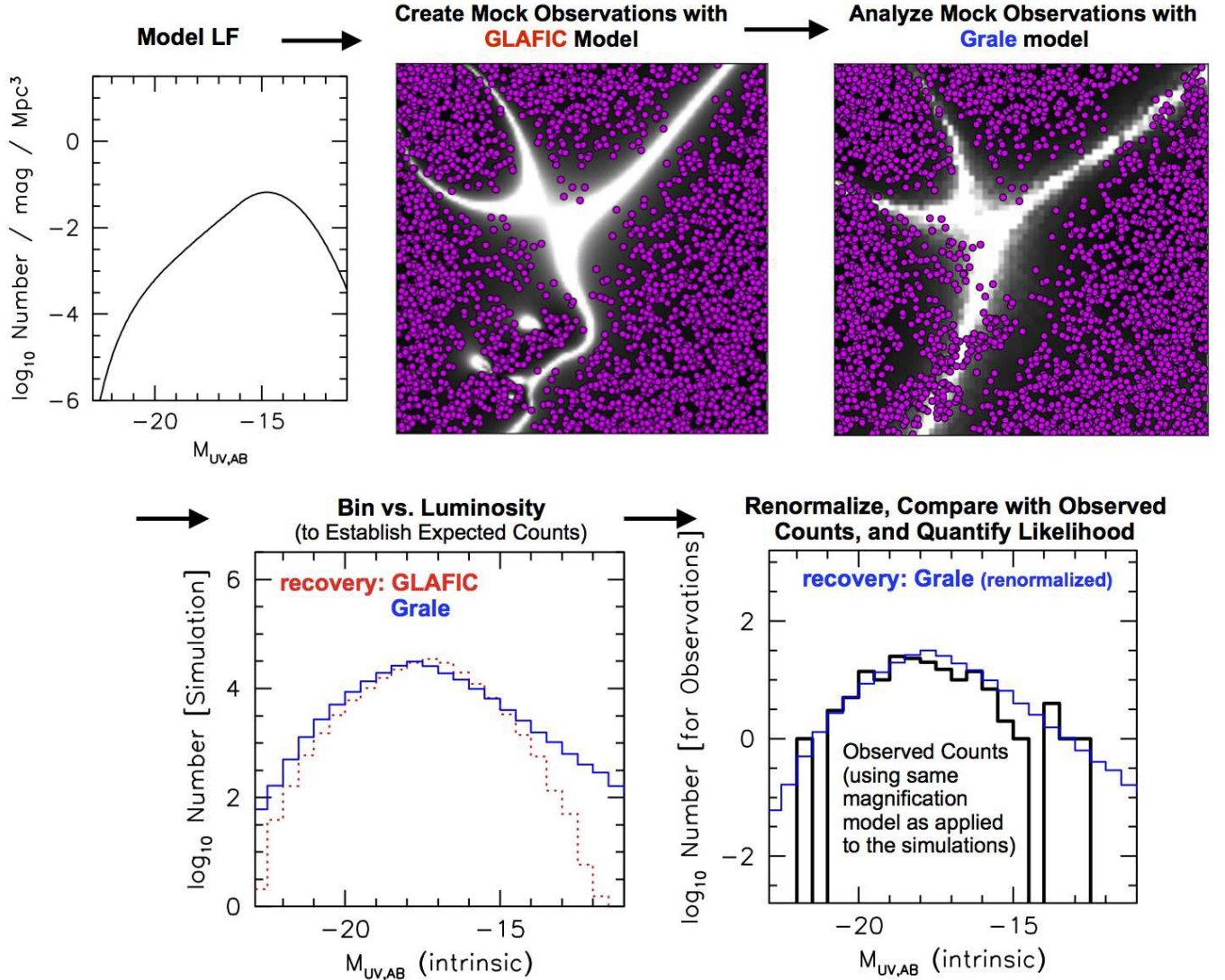


FIG. 5.— Illustration of the steps in our forward-modeling approach to determine the impact of errors in the lensing models on the derived LF results (§4.2: see also §3.2 and §4.1). The upper middle panel shows the positions of the faint $H_{160,AB} > 28$ sources (*violet circles*) from a mock catalog created over a $14'' \times 14''$ region near the center of Abell 2744 based on a model LF (*shown in the upper left panel*) and the GLAFIC lensing model, with the very high magnification regions shown in white. [Note that sources are distributed uniformly over the source plane for the construction of the mock catalog.] The upper right panel shows where this same catalog of sources lies relative to the critical lines in the GRALE lensing model over the same region in Abell 2744. The lower left panel shows histograms of the number of sources in our mock catalogs vs. luminosity, using both the original GLAFIC model used to construct the mock catalogs (*dotted red histogram*) and GRALE model used for recovery (*blue histogram*). We use these simulations to derive the expected number of galaxies per luminosity bin for a given LF and compare this with the observed numbers (where the intrinsic M_{UV} is calculated using the GRALE model) to estimate the likelihood of a given LF model (*lower right panel*). In the presented example, the turn-over in the LF at the faint end translates into a significant deficit of sources near the critical lines using the input magnification model. However, when interpreting this same catalog using a different lensing model, i.e., GRALE in this case, many sources nevertheless lie very close to the critical lines. As a result of the uncertain position of the critical curves, it can be challenging to detect a turn-over in the LF at > -15 mag.

form to extremely low luminosities (as was done by L16 using their Figure 11). The presented examples show this is not a valid argument.

How then can one interpret LF results from lensing clusters when a steep LF $\alpha \sim -2$ is found? As we have demonstrated, such a result could be indicative of the LFs truly being steep or simply an artifact of large magnification uncertainties. To determine which is the case, the safest course of action is to simulate all steps in the LF recovery process, to determine the impact of magnification uncertainties on the shape of the LF, and finally to interpret the recovered LFs from the observations. While we showed a few examples here, we formalize the process

in the next section.

4. NEW FORWARD-MODELING METHODOLOGY TO DERIVE LF RESULTS

The purpose of the present section is to describe a new methodology for quantifying the constraints on the UV LF to very low luminosities, given the uncertainties in the magnification maps. The development of such a procedure is useful given the challenges presented in the previous section. We will apply this formalism in §5.

4.1. Basic Idea and Utility

The LF recovery results presented in §3 (Figure 4) illustrate the impact that errors in the magnification maps

can have on the recovered LFs. Input LFs, of very different form, can be driven towards a faint-end slope α of -2 at the faint end, after accounting for the impact of magnification errors. The results from §3.2 demonstrate the importance of forward modeling the entire LF recovery process to ensure that both the results and uncertainties are reliable.

We then utilize our forward-modeling approach to derive constraints on the $z \sim 6$ LF. The basic idea behind our approach follows closely from the simulations we ran in the previous section and is illustrated in Figure 5. We begin by treating one of the public magnification models as providing an exact representation of reality. In conjunction with an input LF, those models are used to create a mock data set for the four HFF clusters considered. The mock data set is then interpreted using other magnification models for the clusters to determine the distribution of sources vs. UV luminosity M_{UV} and also to recover the UV LF. As illustrated by the LF recovery experiments presented in §3.2, the recovery could be done with the models individually or by using some combination of models like the median.

There are many advantages to using the present procedure to derive accurate errors on the overall shape of the UV LF. Probably the most significant of these is inherent in the end-to-end nature of the present procedure and our relying significantly on forward modeling to arrive at accurate errors on the observational results. Through the construction of many mock data sets using plausible magnification models and recovery using other similarly plausible models, the proposed procedure allows us to determine the full range of allowed LFs.

In addition, the advocated procedure provides us with a natural means to account for “noise” in the lensing model magnification maps. The presence of lensing model “noise” is obvious looking at the range in magnification factors across the various models (e.g., compare the GLAFIC and GRALE critical lines in Figure 5 or see the lower panel in Figure 3). Such noise can even be present in a median magnification model created from the combination of many individual models, as there will be regions where the high-magnification regions of the lensing maps simply overlap due to chance coincidence. Analogous to considerations of low-significance sources in imaging observations, the robustness of specific magnification factors in the median map can be assessed, by considering comparisons with independent determinations of the same map. Through the treatment of one of the public magnification models as the truth, the present forward-modeling approach effectively formalizes such a technique to determine the robustness of specific features in the magnification maps. The advantage of the current procedure is that this robustness can be determined using the full magnification maps available for each cluster (and not just at a limited number of positions where candidate high-magnification $\mu > 10$ sources happen to be found in the real observations), while also allowing us to derive more reliable likelihood distributions (with realistic errors).

Another advantage of our forward modeling procedure is that it explicitly incorporates source selection. This is important, since the selection efficiency S could depend on the magnification factor μ in the sense that the most magnified sources would also be the most incom-

plete, as is likely the case for the brightest and most extended objects, due to the impact of lensing shear on source detection (Oesch et al. 2015). If the same situation applied to the faintest sources in the HFFs (and one did not utilize a procedure that included forward modeling or an explicit correction), the recovered LFs would be biased. This is due to the fact that the actual surface density of the sources on the sky is $S(\mu_{true})$, but it is assumed to be proportional to $S(\mu_{model})$ and $\mu_{true} < \mu_{model}$ at high magnifications $\mu > 10$ (Figure 3). The recovered LF would therefore be higher by the factor $S(\mu_{true})/S(\mu_{model})$.

We would expect such an issue to affect recovered LFs, in all cases where sources have non-zero size (since the selection efficiency would then depend on the magnification factor). For example, if the completeness of sources shows an inverse correlation with the magnification factor as Oesch et al. (2015) find, i.e., $S(\mu) \propto \mu^{-0.3}$ (e.g., as in their Figure 3), a direct approach would recover a faint-end slope that is $\Delta\alpha \sim 0.3$ steeper than in reality (Figure 14 from Appendix B), at very low luminosities where $\mu > 10$ (where $\langle \mu_{true} \rangle$ is typically less than $\langle \mu_{model} \rangle$).

Remarkably, there is no evidence that this issue is even considered in many recently derived LFs, which is worrisome given the size assumptions which were made. This is most problematic for analyses pushing to very low luminosities, i.e., > -15 mag, while quoting tiny statistical uncertainties (e.g., L16 who quote statistical uncertainties on α of ± 0.04 vs. this bias which is $\sim 8\times$ larger).

4.2. Procedure

We perform our forward modeling simulations at the catalog level, to ensure that the time requirements on these simulations are manageable. This involves the construction of catalogs of sources with precise positions and apparent magnitudes. Both in the construction of the mock catalogs and in recovering the LF from these catalogs, the selection efficiency S must be accounted for, which is in general a function of the apparent magnitude m and magnification factor μ , i.e., $S(m, \mu)$. For the lowest luminosity $z \sim 5-8$ galaxies, there is little evidence to suggest that these sources show significant spatial extension (Bouwens et al. 2016), which implies that we can credibly treat their selection efficiencies as just a function of the apparent magnitudes, i.e., $S(m)$. We describe our procedure for estimating $S(m)$ in this case in Appendix A.⁹

In putting together the mock suite of observations for each LF parameter set we are considering, i.e., ϕ^* , α , and a third parameter δ to be introduced in the next section, $\sim 2 \times 10^5$ sources are inserted at random positions (uniformly in the source plane) across the 4 HFF cluster fields we are using (Figure 5). In constructing the mock set of observations, we include sources in the catalogs in proportion to their estimated selection efficiencies $S(m, \mu)$ from Appendix A. All sources in the input catalogs are assumed to have the same input redshift $z = 6$. During the recovery process, sources are placed into individual

⁹ Of course, we also recognize the value in understanding the impact on the results if the sizes of sources are larger, and this is discussed in Appendix B. The outcome is similar but leads to an even bigger disconnect from the real LF shape.

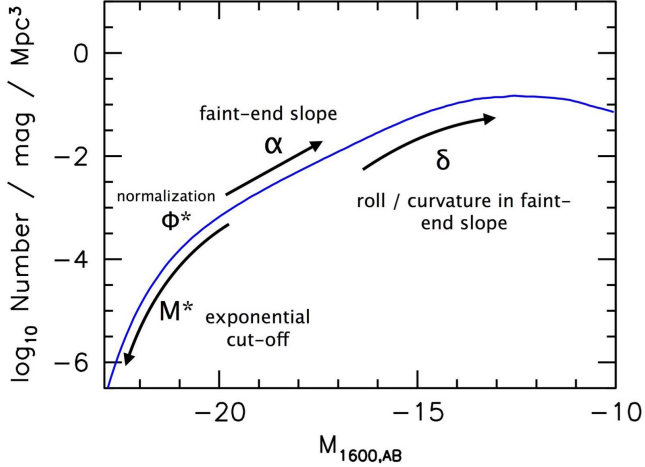


FIG. 6.— Illustration of the parameterization we utilize for the *UV* LF in assessing the possibility it may turn over at low luminosities (§4.3). In addition to the standard Schechter parameters, M^* , ϕ^* , α , we also allow for curvature in the effective slope of the LF using a fourth parameter δ – which can be used either to represent a roll-over or to indicate a possible steepening in the slope towards lower luminosities. We include such a curvature at > -16 mag, coincident with the luminosity range where magnification uncertainties become larger for individual sources. -16 mag also corresponds to that expected for a typically-faint source (~ 28.5 mag) magnified by a factor of 10.

bins in *UV* luminosity using a “recovery” magnification model, which we take to be the median of the parametric magnification models.¹⁰ During the recovery process, the redshift is taken to have the same mean value as assumed in constructing the mock catalogs, i.e., $z = 6.0$, but with a 1σ uncertainty of 0.3. This is to account for the impact of uncertainties in the estimated redshifts of individual sources on the recovered LFs.

We use the results of the simulations we run for each parameter set (each with $\sim 2 \times 10^5$ sources) to establish the expectation values for the number of sources per luminosity bin (in the same 0.5-mag intervals used in the previous section). We then compute the likelihood of a given parameterization of the LF by comparing the observed number of galaxies per bin in luminosity (considering all 4 clusters at the same time) with the expected numbers assuming a Poissonian distribution, as

$$\Pi_i e^{-N_{exp,i}} \frac{(N_{exp,i})^{N_{obs,i}}}{(N_{obs,i})!}$$

where $N_{exp,i}$ is the expected number of sources in a given bin in intrinsic *UV* luminosity. The observed number of sources in a given bin in *UV* luminosity $N_{obs,i}$ is computed from the median parametric magnification maps, as done in §2 (Figure 2). A flow chart showing one example of our forward-modeling approach is provided in Figure 5.

4.3. Parameterization of LF Model

Use of a parametric form to the LF is particularly useful for examining the overall LF constraints on the shape of the *UV* LF in lensed fields, due to uncertainties that

¹⁰ The input magnification model is always excluded when constructing the median magnification map (used for recovery) to keep the process fair.

exist on the magnification factors, and hence luminosities, of individual sources used in the construction of the LF. This makes it difficult to place sources in specific bins of the *UV* LF (resulting in each bin showing a larger error).

For the parametric modeling we do of the LF, we start with a general Schechter form for the LF:

$$\phi^* (\ln(10)/2.5) 10^{-0.4(M-M^*)(\alpha+1)} e^{-10^{-0.4(M-M^*)}}$$

However, we modify the basic form of the Schechter function by multiplying the general Schechter form by the following expression faintward of -16 mag:

$$10^{-0.4\delta(M+16)^2}$$

Positive values of δ result in the LF turning over faintward of -16 mag, while negative values of δ result in the LF becoming steeper faintward of -16 mag. An illustration of this parameterization is provided in Figure 6.

Our use of -16 mag allows us to test for possible curvature in the shape of the LF at > -16 mag, as predicted by some models (e.g., Kuhlen et al. 2013; Jaacks et al. 2013; Ocvirk et al. 2016). -16 mag is also just faintward of luminosities probed in field studies (i.e., -16.77 mag: Bouwens et al. 2015). Finally, since > -16 mag corresponds to the luminosity of $\mu > 10$ faint sources in the HFFs, our fitting for a curvature parameter δ allows us to investigate how well the shape of the LF can be recovered in the regime where the magnification factors are large.

With this parameterization, the turn-over luminosity M_T can be easily shown to be

$$M_T = -16 - \frac{\alpha + 1}{2\delta} \quad (2)$$

assuming that $\delta > 0$.

5. LF RESULTS AT $Z \sim 6$

We now make use of the formalism we presented above and our selection of 160 $z \sim 6$ galaxies behind the first four HFF clusters by R.J. Bouwens et al. (2016, in prep) to set constraints on the form of the *UV* LF at extremely faint magnitudes.

5.1. Using the HFF Observations Alone

We begin by looking at the constraints we can set on the shape of the $z \sim 6$ LF by restricting our analysis to $z \sim 6$ samples found behind the first four HFF clusters. Such an exercise is useful, since it allows us to examine the LF constraints we obtain from our HFF search results, entirely independent of results in the field.

In deriving best-fit LF results, we use the following approach. We fix M^* to the same value Bouwens et al. (2016) found at $z \sim 6$, i.e., -20.94 mag, set the curvature δ to be zero, and then fit for ϕ^* and α . We use a Markov Chain Monte Carlo (MCMC) algorithm where we start with the field LF results from Bouwens et al. (2015), i.e., $\phi^* = 0.0005 \text{ Mpc}^{-3}$ and $\alpha = -1.87$ to determine how the likelihood of various parameter combinations varies as a function of ϕ^* and α . For each set of parameters α and ϕ^* , we repeat the simulations described in §4.2 to calculate the likelihood of those parameters. For those simulation, we consistently use magnification maps from one

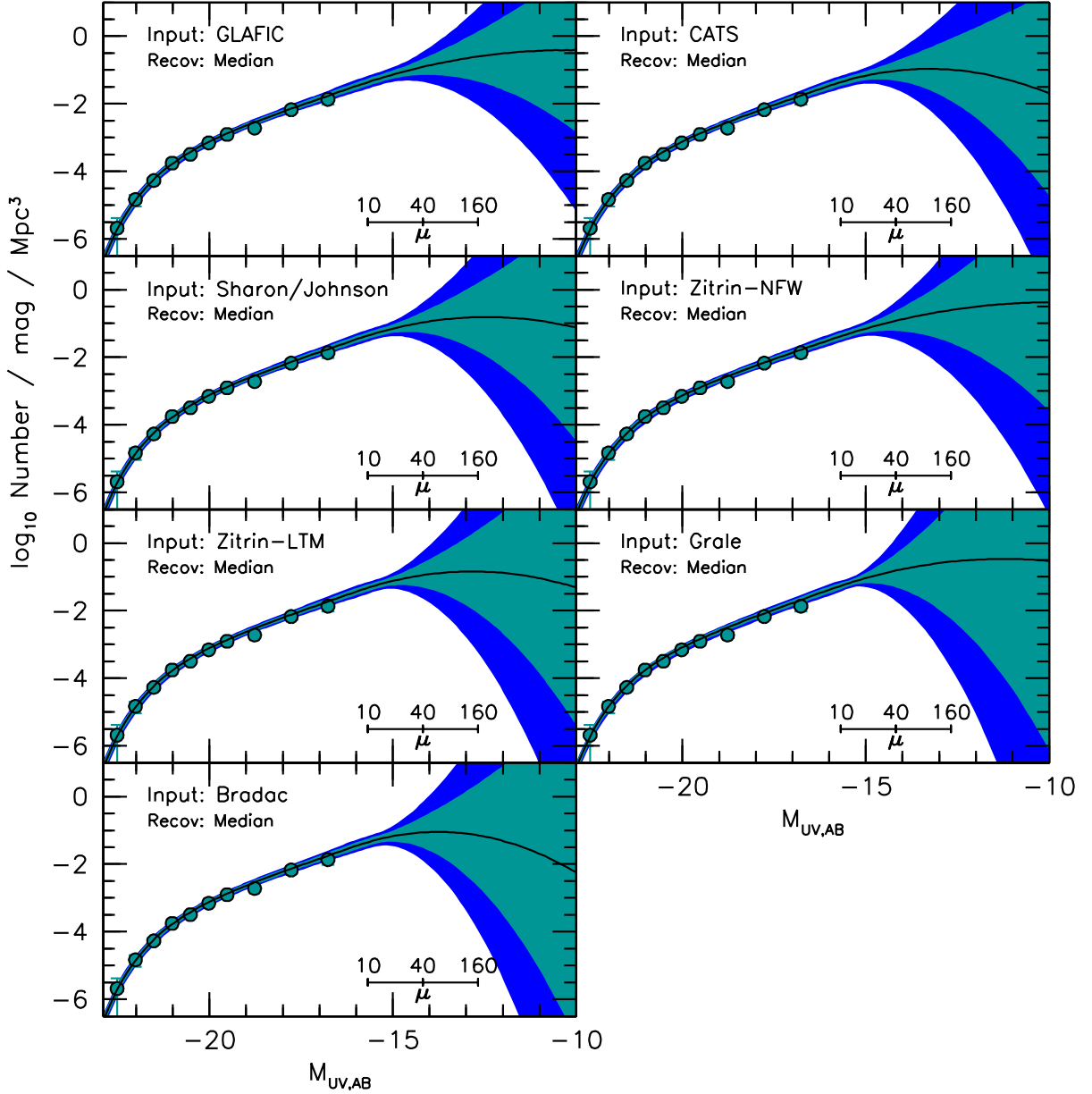


FIG. 7.— Determination of the 68% and 95% confidence intervals (shaded in cyan and blue, respectively: see §5.2) on the overall shape of the $z \sim 6$ LF from the HFF observations alternatively assuming that the GLAFIC, CATS, Sharon/Johnson, Zitrin-NFW, Zitrin-LTM, Bradac, and GRALE lensing models represent reality and recovering the LF using the median of the GLAFIC, CATS, Sharon/Johnson, and Zitrin-NFW models (when available and excluding models from the median when treated as reality to make the assessment fair). The cyan solid circles show the binned $z \sim 6$ LF from the HUDF, HUDF-parallel fields, and CANDELS (Bouwens et al. 2015). The black line indicates the nominal best-fit LF. The ticked line showing the magnification factors is as in Figure 4. The large range of allowed LF (shaded regions) is a direct result of the impact of magnification uncertainties as illustrated in Figure 4. The plotted confidence intervals are tabulated assuming the GLAFIC and Bradac model as inputs in Table 3. If differences between this median magnification map and the non-parametric magnification maps are representative of the actual uncertainties, the present results suggest we cannot rule out a turn-over in the LF at ~ -15 mag. Even taking as the alternate case the assumption that the GLAFIC magnification models represent reality, the present results suggest a turn-over in the LF is permitted at ~ -14.2 mag within the 68% confidence intervals.

team to create the mock observations and then recover the results using the median magnification maps formed from the parametric models. On the basis of the grid of likelihoods we derive, we determine the most likely values for ϕ^* and α , while also determining covariance matrix which best fits the same likelihood grid. From the covariance matrix, we estimate errors on ϕ^* and α .

To determine the impact that errors in the magnification maps can have on the derived values for ϕ^* and α , we repeat the exercise from the above paragraph seven

times. In each case, we treat the magnification maps from a different team as the truth and proceed to derive constraints on ϕ^* and α using the results from the first four HFF clusters. As two of the HFF clusters we examine do not have Zitrin-NFW magnification maps available, i.e., MACS0717 and MACS1149, we make use of the Zitrin-LTM-Gauss models instead. The results are presented in Table 2.

The faint-end slope α results we obtain from the HFF clusters alone inhabit the range -1.89 to -1.98 depend-

TABLE 2
BEST-FIT CONSTRAINTS ON THE $z \sim 6$ UV LF

Input Model	M_{UV}^* ^a	ϕ^* (10^{-3} Mpc $^{-3}$)	α^b	δ^c	M_T^\dagger
HFF Observations Alone + M^* from field LF results (§5.1)					
GLAFIC	-20.94	0.69 ± 0.04	-1.90 ± 0.03	0.00	—
CATS	-20.94	0.66 ± 0.04	-1.91 ± 0.02	0.00	—
GRALE	-20.94	0.68 ± 0.06	-1.98 ± 0.03	0.00	—
Bradac	-20.94	0.70 ± 0.05	-1.89 ± 0.03	0.00	—
Sharon/Johnson	-20.94	0.68 ± 0.04	-1.91 ± 0.02	0.00	—
Zitrin-NFW	-20.94	0.58 ± 0.01	-1.92 ± 0.03	0.00	—
Zitrin-LTM	-20.94	0.67 ± 0.05	-1.95 ± 0.02	0.00	—
Mean	-20.94	0.66 ± 0.06	-1.92 ± 0.04	0.00	—
Mean Parametric	-20.94	0.65 ± 0.06	-1.91 ± 0.03	0.00	—
Fiducial (§5.2): HFF Observations + CANDELS/HUDF/HUDF-Parallel (Bouwens et al. 2015)					
GLAFIC	-20.94	0.57 ± 0.05	-1.92 ± 0.04	0.07 ± 0.16	> -14.2
CATS	-20.94	0.58 ± 0.05	-1.91 ± 0.04	0.17 ± 0.20	> -14.9
GRALE	-20.94	0.63 ± 0.07	-1.95 ± 0.03	0.16 ± 0.30	> -15.2
Bradac	-20.94	0.57 ± 0.05	-1.92 ± 0.04	0.21 ± 0.32	> -15.3
Sharon/Johnson	-20.94	0.57 ± 0.05	-1.92 ± 0.03	0.12 ± 0.21	> -14.9
Zitrin-NFW	-20.94	0.56 ± 0.06	-1.91 ± 0.03	0.07 ± 0.20	> -14.6
Zitrin-LTM	-20.94	0.58 ± 0.05	-1.93 ± 0.03	0.14 ± 0.25	> -15.1
Mean	-20.94	0.58 ± 0.06	-1.92 ± 0.04	0.14 ± 0.24	—
Mean Parametric	-20.94	0.57 ± 0.05	-1.92 ± 0.04	0.11 ± 0.20	—
Idem (but allowing for a larger incompleteness: §5.4)					
GLAFIC	-20.94	0.57 ± 0.05	-1.93 ± 0.04	0.11 ± 0.16	> -14.5
CATS	-20.94	0.57 ± 0.05	-1.93 ± 0.04	0.13 ± 0.19	> -14.8
GRALE	-20.94	0.63 ± 0.07	-1.95 ± 0.03	0.14 ± 0.30	> -15.2
Bradac	-20.94	0.57 ± 0.05	-1.93 ± 0.04	0.17 ± 0.29	> -15.1
Sharon/Johnson	-20.94	0.58 ± 0.05	-1.93 ± 0.04	0.21 ± 0.22	> -15.1
Zitrin-NFW	-20.94	0.56 ± 0.06	-1.92 ± 0.04	0.06 ± 0.19	> -14.4
Zitrin-LTM	-20.94	0.58 ± 0.06	-1.95 ± 0.03	0.16 ± 0.25	> -15.1
Mean	-20.94	0.58 ± 0.06	-1.93 ± 0.04	0.14 ± 0.23	—
Mean Parametric	-20.94	0.57 ± 0.05	-1.93 ± 0.04	0.13 ± 0.20	—
Literature Including HFF Observations					
Atek et al. (2015)	-20.9 ± 0.7	$0.28^{+0.59}_{-0.18}$	$-2.04^{+0.17*}_{-0.13}$	—	—
Livemore et al. (2016)	$-20.82^{+0.04}_{-0.05}$	$0.23^{+0.02}_{-0.02}$	$-2.10^{+0.08}_{-0.03}$	—	$> -11.1^{+0.4}_{-0.8} \ddagger$
Literature Before HFF Observations					
Bouwens et al. (2015)	-20.94 ± 0.20	$0.50^{+0.22}_{-0.16}$	-1.87 ± 0.10	—	—
Finkelstein et al. (2015)	$-21.13^{+0.25}_{-0.31}$	$0.19^{+0.09}_{-0.08}$	-2.02 ± 0.10	—	—

^a Fixed

^b The faint-end slopes we derive are moderately dependent on the assumptions we make about the intrinsic size distribution of very low luminosity galaxies. Nevertheless, motivated by the results from a companion paper (Bouwens et al. 2016) where extremely faint $z \sim 5-8$ galaxies were found to have a size distribution consistent with point sources, we used this assumption in deriving results for the faint end of the UV LF. However, since obtaining direct constraints on the size distribution and hence completeness of extremely faint galaxies over the HFF clusters is difficult, we could underestimate the volume density of faint sources. This could result in faint end slopes that are steeper by $\Delta\alpha \sim 0.15$ (assuming a $2\times$ larger incompleteness than the point-source case).

^c Best-fit curvature in the shape of the UV LF faintward of -16 mag (see Figure 6).

[†] Brightest luminosity at which the current constraints from the HFF permit a turn-over in the $z \sim 6$ LF (within the 68% confidence intervals).

[‡] This is the luminosity where according to Figure 12 of L16, L16 find $\Delta(\text{BIC}) = 2$, where BIC denotes the Bayesian Information Criteria (analogous to $\Delta\chi^2$ for their usage). Strictly speaking, it is closer to a 84% confidence limit than a 68% confidence limit.

* LF constraints obtained for a combined $z \sim 6-7$ sample

ing on which magnification model we treat as reality. The faint-end slope we estimate averaging the results from all of the models is -1.92 ± 0.04 , while the faint-end slope α we find using the parametric models is -1.91 ± 0.03 . The quoted uncertainty includes median statistical error added in quadrature with the standard deviation among the faint-end slope determinations for the different magnification models.

These results are interesting in that they are consistent with our own results over the field, i.e., Bouwens et al. (2015), where $\alpha = -1.87 \pm 0.10$, as well as other estimates

in the literature (Yan & Windhorst 2004; Bouwens et al. 2007; Calvi et al. 2013; Bowler et al. 2015; Finkelstein et al. 2015) which generally lie in the range ~ -1.8 to ~ -2.0 .

It is worthwhile emphasizing the value of the test we perform in the previous paragraph. As we consider the use of searches behind lensing clusters for constraining the faint end of the UV LFs, it is essential that we derive constraints from the lensing clusters in isolation of those obtained from field searches to verify that no major systematics appear to be present in the LF results

TABLE 3
68% AND 95% CONFIDENCE INTERVALS ON
THE UV LF AT $z \sim 6$ (§5.2) ADOPTING THE
FUNCTIONAL FORM IN §4.3

$M_{UV,AB}$	$\phi(M)$ [# / Mpc ³ / mag]			
	Lower Bound 95%	68%	Upper Bound 68% ^c	95% ^c
Case 1 (GLAFIC) ^a				
-16.75	-1.88	-1.82	-1.69	-1.63
-16.25	-1.71	-1.64	-1.50	-1.42
-15.75	-1.54	-1.47	-1.30	-1.23
-15.25	-1.38	-1.30	-1.13	-1.05
-14.75	-1.29	-1.18	-0.95	-0.84
-14.25	-1.31	-1.12	-0.73	-0.54
-13.75	-1.43	-1.13	-0.49	-0.18
-13.25	-1.65	-1.18	-0.22	0.25
-12.75	-1.95	-1.29	0.07	0.73
-12.25	-2.34	-1.45	0.37	1.26
-11.75	-2.82	-1.66	0.70	1.84
-11.25	-3.37	-1.93	1.04	2.48
-10.75	-4.01	-2.24	1.40	3.17
-10.25	-4.74	-2.60	1.79	3.91
Case 2 (Bradac) ^b				
-16.75	-1.85	-1.79	-1.66	-1.60
-16.25	-1.67	-1.60	-1.46	-1.39
-15.75	-1.50	-1.42	-1.27	-1.20
-15.25	-1.34	-1.27	-1.11	-1.04
-14.75	-1.36	-1.21	-0.90	-0.75
-14.25	-1.57	-1.27	-0.65	-0.35
-13.75	-1.93	-1.42	-0.36	0.16
-13.25	-2.43	-1.66	-0.04	0.75
-12.75	-3.08	-1.99	0.31	1.42
-12.25	-3.88	-2.40	0.68	2.18
-11.75	-4.81	-2.90	1.09	3.02
-11.25	-5.88	-3.48	1.52	3.95
-10.75	-7.10	-4.17	1.98	4.95
-10.25	-8.46	-4.93	2.47	6.04

^a For case 1, we assume that differences between the magnifications in the median parametric model and the GLAFIC model are a good representation of the typical errors in the magnification models we utilize.

^b For case 2, we assume that differences between the magnifications in the median parametric model and the Bradac model are a good representation of the typical errors in the magnification models we utilize. Similar confidence regions are obtained if one uses the GRALE model instead of the Bradac model.

^c If 50% of faint sources at $z \sim 6-8$ are significantly spatially extended (intrinsic half-light radii >30 mas), the 68%-likelihood upper bounds on the implied LF constraints could increase by ~ 0.3 dex (Bouwens et al. 2016). The 95%-likelihood upper bound could increase by as much as ~ 0.6 dex.

from the lensing clusters. This is relevant, since recent determinations of the faint-end slope α to the LFs from field and cluster search results seem to show a substantial discrepancy (Figure 1).

We should emphasize however that the uncertainties on the faint-end slope α we quote, i.e., ± 0.03 or ± 0.04 , are the formal statistical errors and likely smaller than the true errors, which also include systematic uncertainties. One particularly important systematic uncertainty regards the dependence of the LF results on the unknown size distribution, through the incompleteness effects (e.g., Bouwens et al. 2016; Grazian et al. 2011). If the sizes of faint galaxies are sufficiently different from point sources such that the completeness is overestimated by a factor of 2, the faint-end slope we

derive would be too shallow by $\Delta\alpha \sim 0.15$.

5.2. Using results from the HFF clusters and the field

We now proceed to derive constraints on the overall form of the UV LF at $z \sim 6$ combining constraints from the field with those available from the HFF clusters. For simplicity, we keep the characteristic luminosity M^* fixed to the value -20.94 mag that we found in our earlier wide-area field study (Bouwens et al. 2015), given the lack of substantial information in the HFF cluster program for constraining this parameter due to the small volume probed.

In combining constraints from the field and from the HFF clusters, we need to allow for some error in the normalization of both the field and HFF cluster results, as a result of large-scale structure variations (“cosmic variance”: Robertson et al. 2014; see also Somerville et al. 2004 and Trenti & Stiavelli 2008) and also small systematic errors in the estimates of the volume densities of galaxies in each of our probes. We assume an uncertainty of $\sim 20\%$ in the volume density in both the field and HFF LF results.

The 20% uncertainty we assume to be present in the normalization of the LF results at both the bright and faint ends includes a $\sim 10\%$ uncertainty in our estimates of the selection volume and $\sim 10\%$ systematic error due to uncertainties in the total magnitude measurements (reflecting a ~ 0.1 mag systematic error in the magnitude measurements). The inclusion of such an error is relevant given the existence of real errors in the estimated volume densities of galaxies using photometric criteria. Small differences appear to be guaranteed, given that the filters available for the selection of galaxies from the field are different (in particular including a deep “z”-band filter) from those available over the HFF clusters (which do not include a deep “z” band filter). Important factors contributing to these uncertainties are (1) likely differences between the assumed sizes and SEDs of galaxies vs. redshift in the observations vs. those in the simulations and (2) uncertainties in the contamination rate of observed samples.¹¹

Similar to our LF results using the HFF observations alone, we derive confidence regions on the $z \sim 6$ LF results using a MCMC-type procedure where we explore a limited region in parameter space $\phi^*-\alpha-\delta$ space and calculate the likelihood of each point in parameter space using the forward modeling simulations we describe in §4.1. Our calculated likelihoods explicitly include a marginalization across the 20% volume density uncertainties we assume. These likelihoods are then multiplied by the likelihoods on the same Schechter parameters derived by Bouwens et al. (2015) at $z \sim 6$ using results from the full CANDELS program, the HUDF, and the HUDF parallels (again after marginalizing the Bouwens et al. 2015

¹¹ Measurements of the total magnitudes typically differ at ~ 0.1 mag level, as evident looking at the broad range of magnitude measurements in Skelton et al. (2014). See e.g. their Figures 35-36. The situation is likely even more challenging for galaxies behind lensing clusters due to the substantial foreground light from the clusters themselves, and in fact the total magnitudes measured with different procedures and by different groups are found to differ at the ~ 0.2 mag to 0.25 -mag level. See §6.1.2. This translates into normalization differences of $\sim 20\%$ to $\sim 25\%$ assuming a faint-end slope of ~ -2 for LF results.

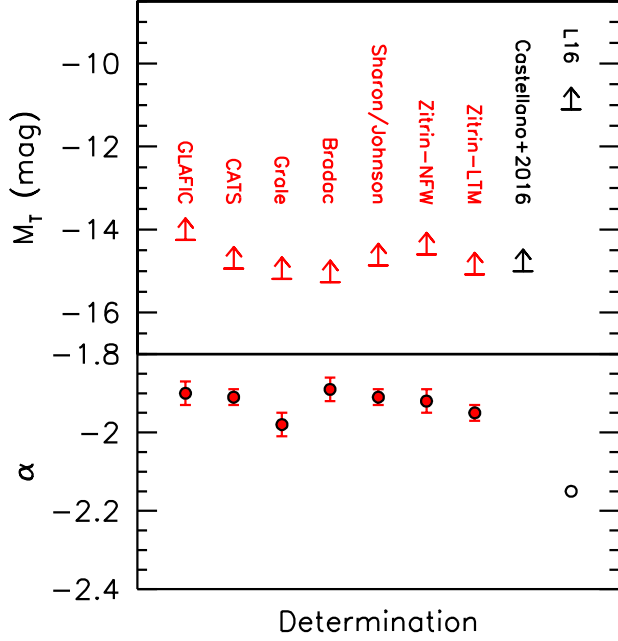


FIG. 8.— (*upper*) Brightest luminosity allowed for a potential turn-over in the $z \sim 6$ UV LF (within our 68% confidence intervals), using faint $z \sim 6$ galaxies identified behind the first four HFF clusters and assuming different magnification models represent reality. The reported constraints from Castellano et al. (2016) and L16 are also presented, with the L16 constraints plotted at a $\Delta(\text{BIC})$ value of 2. The substantially fainter allowed turn-over luminosity reported by L16 (significantly discrepant with the other estimates) is likely an artifact of the very large sizes L16 assume (see Figure 10, §6.1.2, §6.2, and also Bouwens et al. 2016). (*lower*) Faint-end slope α determinations using only the HFF cluster search results. See Table 2 for a tabulation of these results.

over ϕ^* to account for a 20% uncertainty in the volume density of sources). Finally, this 3D likelihood grid is fit to derive the most likely values for ϕ^* , α , and δ and also the covariance matrix.

As in our determinations of the LF parameters from the HFF programs alone, we repeat this exercise seven different times, treating each of the magnification models from different teams as reality and recovering the LF results using the median magnification map. We present our constraints on each of the LF parameters in Table 2. The faint-end slope α we estimate averaging all of our models and just the parametric models are -1.92 ± 0.04 and -1.92 ± 0.04 , respectively.

As in our determinations using only the HFF observations themselves, the faint-end slopes α we derive at $z \sim 6$ are fairly consistent with LF results in the field. Our obtaining consistent results for all seven of the magnification model families we consider is not especially surprising, given the fact that individual sources would be expected to scatter in almost the same direction as the dominant slope of the LF, i.e., ~ -2 (the expected slope of the LF from scatter) vs. ~ -1.9 (the actual slope of the LF).

Despite general agreement on the most likely value for α at $z \sim 6$, we find a broad range of values for the curvature parameter δ , from 0.07 to 0.21, with 1σ uncertainties ranging from 0.16 to 0.32. None of the magnification models we considered point towards our having

TABLE 4
68% AND 95% CONFIDENCE INTERVALS ON THE UV
LUMINOSITY DENSITY AT $z \sim 6$ TO VARIOUS LIMITING
LUMINOSITIES (§5.5)

	$\log_{10} \rho_{UV}$ (UV Luminosity Density) ($\text{ergs s}^{-1} \text{ Hz}^{-1} \text{ Mpc}^{-3}$)			
	Faint-End Limit	Lower Bound 95%	Upper Bound 68%	95%
Case 1 (GLAFIC) ^a				
$M_{UV} < -17$		26.13	26.17	26.25
$M_{UV} < -15$		26.28	26.33	26.42
$M_{UV} < -13$		26.35	26.40	26.54
$M_{UV} < -10$		26.36	26.42	26.93
$M_{UV} < -3^b$		26.36	26.42	31.10
Case 2 (Brodac) ^a				
$M_{UV} < -17$		26.13	26.18	26.26
$M_{UV} < -15$		26.29	26.33	26.43
$M_{UV} < -13$		26.33	26.39	26.57
$M_{UV} < -10$		26.33	26.39	27.39
$M_{UV} < -3^b$		26.33	26.39	34.35

^a Same assumptions as in Table 3.

^b The -3 mag limit is included here for illustrative value and takes as its inspiration results from O’Shea et al. (2015) and Ocvirk et al. (2016) which predict sources to such faint magnitudes.

even modest evidence, i.e., $> 2\sigma$, for the $z \sim 6$ LF showing a turn-over at the faint end.

We find the smallest uncertainties on δ assuming that the GLAFIC magnification models represent reality. Slightly larger uncertainties on δ are found assuming that the CATS, Sharon/Johnson, and Zitrin-NFW models represent reality, while the largest uncertainties on δ are found, assuming that the Zitrin-LTM, Brodac, and GRALE models represent reality. The size of the uncertainty on δ is a function of how similar the various magnification models are to the median magnification model formed from the parametric models. Given the similarity of assumptions utilized in the GLAFIC, CATS, Sharon/Johnson, and Zitrin-NFW models, it is not surprising that their magnification maps agree best with median magnification maps constructed using similar assumptions.

The results in Table 2 for the different magnification models indicate the general range of constraints one could obtain on the form of the $z \sim 6$ LF: the results for the non-parametric models indicate the errorbars on the LFs if the mass distribution in clusters do not strictly follow the assumptions made in the parametric models, while results for the parametric models indicate the likely error bars, if the mass profiles in the HFF clusters generally do adhere to those assumptions.

Uncertainties in the redshifts of the lensed $z \sim 6$ galaxies also contribute to the error in δ . To estimate the impact, we kept the redshifts of lensed background sources fixed while rerunning the forward-modeling simulations from our MCMC chain. Comparing the uncertainties we derive in δ to the uncertainties we derive including errors in the redshift, we find a typical decrease of 0.01 in the uncertainty on δ , i.e., from 0.16 to 0.15 in the case of the GLAFIC simulations.

To help visualize what our present LF results mean, we have made use of our parametrized constraints to derive 68% and 95% confidence intervals on the volume density of galaxies as a function of the UV luminosity

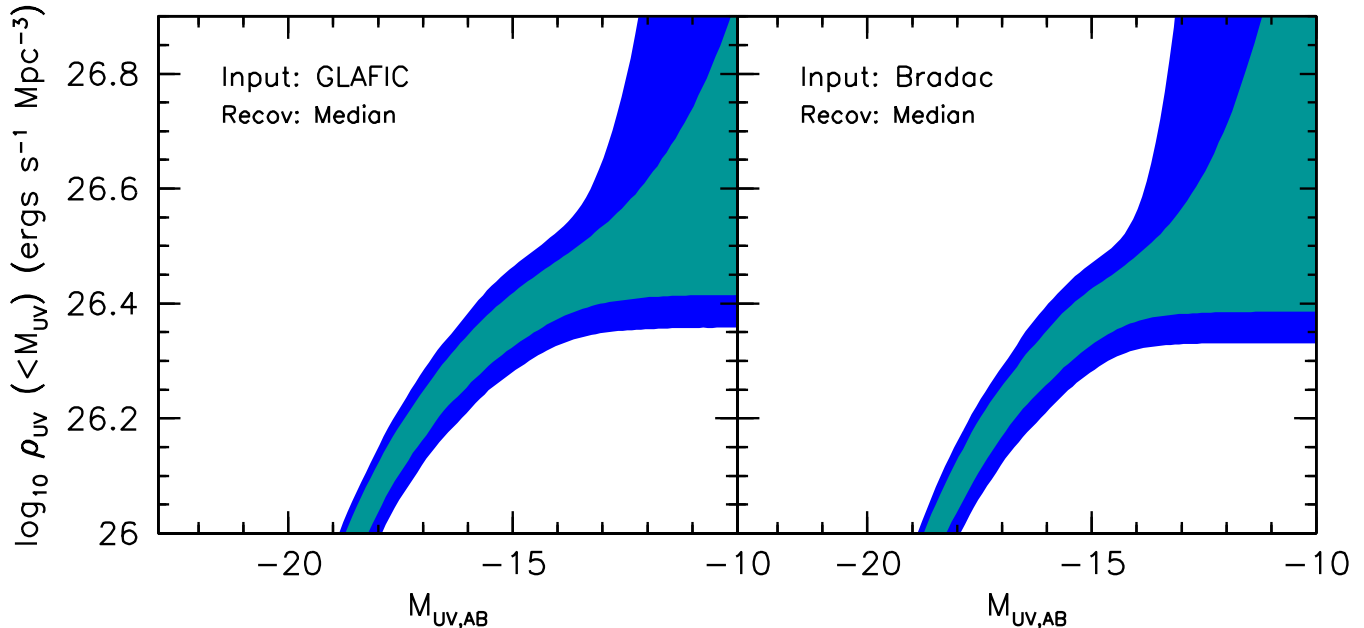


FIG. 9.— 68% and 95% confidence intervals (shaded in cyan and blue, respectively) on the estimated UV luminosity density for all sources brighter than some M_{UV} (§5.5). Shown are the results for two different assumptions about the size of the magnification errors in the lensing models. As we integrate further down the UV LF to derive the luminosity densities, the lower boundaries allowed by our analysis show a clear monotonic increase. However, faintward of ~ -15 mag, the lower boundaries cease to show an increase that is highly significant (i.e., $>1.5\sigma$). This demonstrates that it is not yet possible to make strong claims that > -15 mag galaxies provide an additional reservoir of photons to reionize the universe.

M_{UV} . These results are presented both in Figure 7 and also in Table 3.

5.3. Constraints on a Possible Turn-Over in the $z \sim 6$ LF

One question that has recently been of significant interest in the literature regards whether there is a flattening or turn-over in the UV LF at the faint end. This question is important, since the answer could indicate to us whether there is a sufficient number of extremely faint galaxies to produce the photons necessary for driving the reionization of the universe.

Fortunately, using the likelihood contours for δ - α - ϕ^* and Eq. 2, we can directly determine the brightest point in the LF where a turn-over is permitted (with the 68% confidence intervals). The results do depend somewhat on which magnification model we assume to be representative of reality (and therefore which of the panels we consider from Figure 7). Nevertheless, we find that the HFF observations allow for a turn-over in the LF as bright as -14.2 mag to -15.3 mag (within the 68% confidence intervals). The allowed turn-over luminosities we estimate assuming different magnification models are presented in Table 2 and also in Figure 8.

5.4. LF Results (Including an Allowance for a $2\times$ Larger Incompleteness)

Besides the lensing models, the unknown sizes of extremely faint $z \sim 6$ galaxies represents a potentially significant uncertainty for constraints on the $z \sim 6$ LF. If a modest fraction of faint, highly-magnified galaxies behind HFF clusters had intrinsic half-light radii of $>0.06''$,

the successful detection of these sources would be challenging.

In a companion paper (Bouwens et al. 2016), we looked into the question of the intrinsic sizes of extremely faint galaxies, taking advantage of the large samples of extremely faint, highly magnified $z \sim 2-3$ + $z \sim 5-8$ galaxies available behind the first four HFF clusters. We found no evidence to indicate that these galaxies were resolved, looking at (1) the prevalence of high magnification sources as a function of the predicted shear and (2) their stacked profile along the expected shear axis.

However, the absence of evidence for extended faint galaxies behind the HFF clusters is not itself an indication (or evidence) that such extended sources do not exist. The size distribution could be bimodal or show an extended tail towards large values.

One admittedly ad hoc way of accounting for the unknown size distribution is to suppose that our completeness estimates using point sources could be up to a factor of 2 too low, e.g., as we would derive if $\sim 50\%$ of the very faint (> -16.5 mag) sources in our samples had sizes of ~ 50 mas or larger. This contrasts with the other case that we consider, where we have assumed that our completeness estimates, using point sources, are accurate. Given that we do not know which is the case, we repeat our determinations of the LF parameters from the previous section, but now include another step in the process where we marginalize our likelihood estimates over the unknown completeness of our faint sample (assuming a uniform prior on the completeness lying somewhere between 50% and 100% of the point source case).

These results are presented in Table 2. The results are fairly similar to our fiducial results but give faint-end slopes α that are $\Delta\alpha \sim 0.01-0.02$ steeper. As specified

TABLE 5
BINNED DETERMINATION OF THE
REST-FRAME UV LF AT $z \sim 6$ (§5.6)[†]

$M_{UV,AB}$ ^a	ϕ_k (10^{-3} Mpc $^{-3}$ mag $^{-1}$)
−20.75	0.0002±0.0002
−20.25	0.0009±0.0004
−19.75	0.0007±0.0004
−19.25	0.0018±0.0006
−18.75	0.0036±0.0009
−18.25	0.0060±0.0012
−17.75	0.0071±0.0014
−17.25	0.0111±0.0022
−16.75	0.0170±0.0039
−16.25	0.0142±0.0054
−15.75	0.0415 ^{+0.0083} _{−0.0069} ^b
−15.25	0.0600 ^{+0.0128} _{−0.0106} ^b
−14.75	0.0817 ^{+0.0283} _{−0.0210} ^b
−14.25	0.1049 ^{+0.0743} _{−0.0435} ^b
−13.75	0.1270 ^{+0.1817} _{−0.0748} ^b
−13.25	0.1451 ^{+0.4114} _{−0.1073} ^b
−12.75	0.1567 ^{+0.8885} _{−0.1332} ^b

[†] These LF results are simple estimates, representing the # of sources at a given luminosity (using the median magnification maps) after division by the selection volumes. No account is made for scatter resulting from errors in the magnification maps. Errors in the magnification maps can be best handled using the forward modeling simulations and methodology we consider in §4.2, leading to the results presented in Table 3.

^a Upper limits are 1σ .

^b 68% confidence intervals on the $z \sim 6$ UV LF at > -16 mag we achieve using forward modeling and observations of the first four HFF clusters in §4.3. The quoted constraints give the geometric mean of our results using the GLAFIC, CATS, and Sharon/Johnson parametric models as inputs. The error bars are not independent.

earlier in this section, if we assume that our completeness estimates are a factor of 2 too high and ignore the field results, we derive a faint-end slope which is steeper by $\Delta\alpha \sim 0.15$.

5.5. Implied Constraints on the $z \sim 6$ UV Luminosity Density

To determine if galaxies produce enough ionizing photons to drive the reionization of the universe, we require constraints on the luminosity density in the rest-frame UV that include the contribution from all galaxies.

We can compute confidence intervals on the luminosity densities in the rest-frame UV by using the constraints from the analyses performed in the previous section and then marginalizing over ϕ^* , α , and δ . We compute the results to a number of different limiting luminosities M_{UV} , i.e., -17 mag, -15 mag, -13 mag, -10 mag, and -3 mag,¹² the first four of which commonly appear in the literature, in considering whether galaxies might drive cosmic reionization, particularly including the contribution at very low luminosities. We have presented the

¹² The faintest limit here, -3 mag, is only included for illustrative value and takes as its inspiration results from O’Shea et al. (2015) and Ocvirk et al. (2016) which predict sources to such faint magnitudes.

results we obtain in Figure 9 and also in Table 4 to these faint-end limits. Our results imply a luminosity density of $10^{26.38 \pm 0.05}$ ergs s $^{-1}$ Hz $^{-1}$ Mpc $^{-3}$ to -15 mag.

Not surprisingly, our LF results allow for essentially an arbitrarily high contribution from very faint galaxies to the UV luminosity density, particularly including a contribution from galaxies to -3 mag. These results also provide fairly firm 1σ and 2σ lower bounds on our results. We find 1σ and 2σ lower limits on luminosity density in the rest-frame UV of $\sim 10^{26.40}$ ergs s $^{-1}$ Hz $^{-1}$ Mpc $^{-3}$ and $\sim 10^{26.35}$ ergs s $^{-1}$ Hz $^{-1}$ Mpc $^{-3}$, respectively.

The 1σ and 2σ lower bounds we find on the luminosity density integrating to arbitrarily faint luminosities is not especially higher than what we find integrating to -15 mag. These results indicate that it is not yet possible to argue for the discovery of a significant additional reservoir of photons from galaxies faintward of -15 mag (Atek et al. 2015a,b), as has been the claim in one recent study (L16).

5.6. Binned Determinations of $z \sim 6$ LF Using Direct Method

Finally, to conclude this section, we derive a binned representation of the results from the first four HFF clusters. Binned representations of the LF results from the HFFs should be very reliable at high luminosities, where errors in the magnification maps are smaller. Binned representations retain the advantage that they are a much more model independent probes of the LF shape as a function of luminosity.

In our binned representation of the LF, we adopt bins of width 0.5 mag and determine the binned LF results ϕ_m to be as follows:

$$\phi_m = \frac{N_m}{V_m} \quad (3)$$

where N_m is the number of sources in absolute magnitude bin m after correcting for the estimated magnification.

We derive the selection volumes V_m in a given magnitude bin using the following equation:

$$V_m = \int_A \int_{dz} C(z, m, \mu) \frac{1}{\mu(A)} \frac{dV(z)}{dA} dz dA \quad (4)$$

where A denotes the area, V denotes the volume, C denotes the estimated completeness, and μ denotes the magnification factor. Our estimates of the completeness are provided in Appendix A; the completeness C appears not to be a strong function of the magnification factor μ in data sets as deep as the HFFs (see Bouwens et al. 2016).

We derived simple stepwise constraints on the UV LF brightward of -16 mag, by dividing the number of sources in each absolute magnitude bin by the computed selection volume. The results are presented in Table 5 and Figure 10. Faintward of -16 mag, we include results in Table 5 and Figure 10 by taking the geometric mean of the best-fit LF results using the GLAFIC, CATS, and Sharon/Johnson models. We present those results to luminosities plausibly probed by the present study. 1σ errors on the results at the faint end of the $z \sim 6$ LF are similarly taken to be the geometric mean of the confidence intervals on the LF fits for the same parametric magnification models.

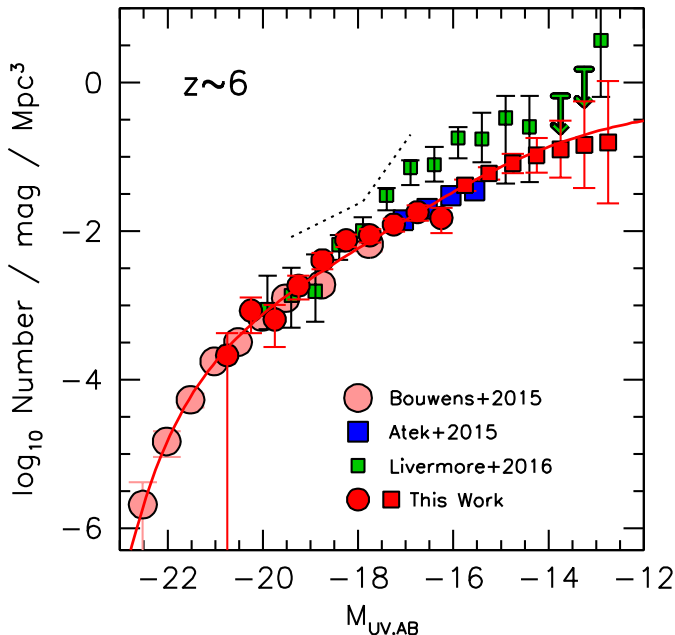


FIG. 10.— Comparison of the present stepwise UV LF at $z \sim 6$ (dark red circles: see §5.6) with previous determinations by Atek et al. (2015: blue squares), L16 (green squares), and Bouwens et al. (2015) using the HUDF, HUDF-parallel, and CANDELS fields (light red circles). All error bars and upper limits are 1σ . The dark red squares give the results from our full forward-modeling procedure, as given in §4 (but where the error bars are not independent: see §5.6). See Table 5 for a tabulation of the present constraints shown here. The red line shows our best-fit LF that we derive by doing a forward-modeling analysis using the GLAFIC magnification models as inputs. The luminosities of the individual points in the L16 and Atek et al. (2015) LFs have been corrected brightward by ~ 0.4 mag and ~ 0.3 mag, respectively, to ensure better consistency with the luminosities (and total magnitudes) measured in our own study (see §6.1.2). The dotted green line shows the feature in the $z \sim 6$ LF results of L16 (i.e., an apparent steepening) that likely drives their claiming no turn-over in the $z \sim 6$ LF until -11 mag (see §6.2).

6. DISCUSSION

The purpose of this paper is to present new constraints on the form of the $z \sim 6$ LF to low luminosities utilizing new constraints from the first four clusters available from the HFF program.

6.1. Comparison with Previous Observational Constraints

Before looking into comparisons of our new observational constraints with theory, it is useful first to compare the present results with previous results where available to try to understand differences where they might occur.

6.1.1. Atek et al. (2015)

We first consider a comparison with the most recent results of Atek et al. (2015) who make use of observations available over the first three HFF clusters Abell 2744, MACS0416, and MACS0717 and selected galaxies using an I_{814} -dropout selection criteria which would identify galaxies from $z \sim 6$ to $z \sim 7$.

A comparison with the most recent determination of the $z \sim 6$ -7 LF from Atek et al. (2015) is provided in Figure 10. In comparing against the Atek et al. (2015) LF determinations, we incorporate a ~ 0.3 -mag brightward

shift of the Atek et al. (2015) LF to correct for differences in our apparent magnitude measurements for individual sources. As already noted in one of the companion papers to this study (Bouwens et al. 2016), overall the agreement appears to be quite good, at least insofar as the stepwise points are concerned.

The best-fit ϕ^* and luminosity density that Atek et al. (2015) estimate to -15 mag, i.e., $\sim 10^{26.20 \pm 0.13}$ ergs s^{-1} Hz^{-1} Mpc^{-3} , is ~ 0.18 dex lower than what we find. This is a small but readily understandable difference that arises because Atek et al. (2015b) provide a constraint on the LF at a higher mean redshift than we do, i.e., $z \sim 6.5$ vs. $z \sim 6$, and also include in their determinations results from field surveys, i.e., CANDELS or the HUDF, which probe $z \sim 7$ vs. our $z \sim 6$ probe. Given that the integrated luminosity density to a limit of -17 mag changes by ~ 0.2 dex per unit redshift, our larger luminosity density estimate is entirely expected.

6.1.2. L16

To ensure that comparisons with the LF results from L16 were made using a consistent luminosity scheme, we carefully cross-matched sources from our catalogs with those from L16 and comparing our measured apparent magnitudes with those inferred from their study using the tabulated absolute magnitudes, redshifts, and magnification factors.

Comparing the total magnitudes we infer for sources using our scaled aperture scheme to the L16-inferred magnitudes, we find a 0.52-mag median difference, with L16-inferred magnitudes fainter than ours, both for relatively bright $H_{160,AB} < 28$ sources and fainter $H_{160,AB} > 28$ sources. If we instead estimate total magnitudes for sources by taking the flux in fixed apertures that would enclose 70% of the flux for point sources, as performed by HUDF12 team (Schenker et al. 2013; McLure et al. 2013) and derive an inverse variance-weighted total magnitude from the Y_{105} , J_{125} , JH_{140} , and H_{160} bands, we find differences of 0.25-mag in the median, with the L16-inferred magnitudes being fainter, comparing magnitudes for the faintest sources (i.e., > 28 mag). The L16 magnitudes show a similar offset relative to the published photometry of Atek et al. (2015a).

Given that the HUDF12 apparent magnitude measurement scheme should give a fairly conservative lower limit on the total fluxes for individual candidates, these comparisons suggest that L16 systematically underestimate the luminosity of individual sources in their catalog by at least ~ 0.25 mag, if not more (taking our scaled-aperture magnitudes as the baseline). In the next subsection, we present evidence that L16 underestimated the flux in the faintest $z \sim 6$ candidate (in this case by ~ 1 mag).

Given this range in values, we adopt a shift of the binned $z \sim 6$ LF of L16 brightward by 0.4 mag to compare volume density measurements at luminosities closer to what we measure. After doing so, we find that the L16 stepwise results appear to be a factor of ~ 3 - $4\times$ higher than our own results in the luminosity range -17 to -14.5 mag (Figure 10). After considering different explanations for these differences, it would appear that they are due to the large intrinsic half-light radii that L16 assume (median of $0.09''$). In Bouwens et al. (2016), we demonstrated through extensive simulations that such size assumptions would result in much higher inferred

volume densities for sources (by factors of >5) than if smaller sizes (i.e., <10 mas) were assumed. See Figure 2 from Bouwens et al. (2016).

With our recent paper (Bouwens et al. 2016; see also Kawamata et al. 2014; Laporte et al. 2016), it is now clear that the use of such large sizes is not realistic. Several lines of evidence indicate that the intrinsic half-light radii of very low luminosity sources (i.e., > -16 mag) are very small, i.e., $\lesssim 0.03''$, with many sources appearing to have sizes $\lesssim 0.01''$ (Bouwens et al. 2016). Small sizes imply small incompleteness corrections and therefore much lower volume densities for faint galaxies. It is important to verify that the sizes assumed in selection volume simulations are realistic, given how sensitive the selection volume estimates (and hence LF) for faint galaxies are to this issue (see Figure 11 of Bouwens et al. 2016).

The very high volume densities L16 find for > -17.5 mag galaxies in their $z \sim 6$ LF likely impacted the analyses they performed regarding a possible turn-over at the faint end, as we explain in §6.2. It would be very difficult for L16 to find evidence for a brighter turn-over being allowed, if one considered LF results that included an apparently steepening slope at -17 mag (see dotted feature in Figure 10).

For similar reasons, the present constraints on the faint-end slope α , i.e., $\alpha = -1.92 \pm 0.04$ are shallower than obtained by L16. Given that the constraints can potentially depend on the gravitational lensing model assumed, it is perhaps best to compare faint-end slopes assuming the same gravitational lensing model. If we take their formal constraints as measured assuming the GLAFIC gravitational lensing model, our estimated faint-end slope α is -1.92 ± 0.04 vs. the L16 faint-end slope at $z \sim 6$ of -2.10 ± 0.03 , a difference of 3.5σ .

The actual differences between our faint-end slope α estimates and L16's estimates are likely even larger than 3.5σ , given that L16 combine their HFF measurements with the Finkelstein et al. (2015) field constraints which prefer -2.02 . Re-estimating the faint-end slope α from the L16 HFF results alone, we infer faint-end slopes of -2.15 to -2.3 (see Appendix D here or §6.2 of Bouwens et al. 2016). This is significantly ($\geq 4.5\sigma$) steeper than our mean estimate using the HFF data alone -1.92 ± 0.04 .

6.2. Observational Constraints on a Possible Turn-over at Very Low Luminosities

One issue we examined in this study concerned the existence of a possible turn-over in the $z \sim 6$ UV LF at the faint end.

Since we could not find compelling evidence for a turn-over at the faint end of the LF (§5.3), we proceeded to examine what constraints we can place on the presence of a turn-over as well as the luminosity at which a turn-over could occur. Using our search results, we concluded that any possible turn-over in the LF would need to occur at $\gtrsim -14.2$ mag or $\gtrsim -15.3$ mag (within the 68% confidence intervals), depending on the assumptions we made about errors in the magnification maps.

The present conclusions seem fairly similar to the findings of Castellano et al. (2016b), who had previously concluded that the UV LF at $z \sim 6$ appeared unlikely to show a turn-over at < -15 mag (68% confidence), after factoring in the uncertainties in the magnification maps.

L16 had concluded based on their analysis of $z \sim 6$ galaxies behind the first two HFF clusters that they have “positive” and “strong” evidence that any turn-over in the LF must be fainter than -11.1 mag and -12 mag, respectively, using the criteria $\Delta(\text{BIC}) = 2$ and $\Delta(\text{BIC}) = 6$, respectively (where we draw these numbers from their Figure 12). BIC denotes the Bayesian Information Criterion (Schwarz 1978). Given their application of BIC, BIC is effectively just equal to $\Delta\chi^2$, and the above limits on the turn-over luminosity translate to nominal confidence levels of 84% and 98.5%, respectively. On the basis of the L16 fit results assuming different magnification models, L16 reported an uncertainty in their allowed turn-over luminosity of $^{+0.4}_{-0.8}$ mag and $^{+0.3}_{-0.6}$ mag, respectively. While our conclusions regarding the lack of a bright turnover do not impact the L16 claim, there are other reasons for being concerned about the validity of their turn-over constraints and their claim that it cannot occur at brighter magnitudes.

L16 claimed evidence against a turn-over in the $z \sim 6$ LF 3.1 mag fainter than what we do (taking the GLAFIC-vs.-median magnification map uncertainties to be typical), despite their examining just half the present data set and with a smaller $z \sim 6$ sample. How could they claim stronger constraints? Remarkably, we believe the reason lies not in the faintest source they report, but instead in the very high volume densities they estimate for the UV LF in the range -17 to -15 (which lie in significant excess of our own determinations, by factors of ~ 3 -4: see Figure 10).

When compared to brighter points in the LF, the volume density of sources they report over the luminosity range -17 to -15 is sufficiently high (and possessing such small error bars) as to suggest a LF form which steepens further at lower luminosities, i.e., $\delta < 0$, rather than one which retains a fixed faint-end slope and then flattens towards lower luminosities, i.e., $\delta > 0$ (using our formalism). Given the inclusion of these points, with a “concave up” feature at ~ -17 mag (*indicated in Figure 10 with the short dotted line feature*), in their LF fits, we suspect it would be very difficult indeed for L16 to find evidence for a turn-over at intermediate luminosities (since all the “evidence” would seem to point in the opposite direction). Given the statistical weight of this feature at ~ -17 to -15 mag and the points brighter than -17 mag, L16 would find that they needed to probe very faint indeed to find a luminosity where a turn-over was allowed.

Even if we ignore such issues, L16 present a second piece of evidence to argue against a possible turn-over at ~ -15 mag and this involves a $z \sim 6$ candidate reported to be at ~ -12.4 mag and on whose basis they estimate a volume density of ~ 6 galaxies per Mpc^3 at ~ -12.5 mag. If robust, this candidate could also argue against a turn-over in the LF at higher luminosities.

This $z \sim 6$ candidate from L16 is also detected in our catalogs. However, it fails to meet our selection criteria, due to the fact that the integrated likelihood of the candidate lying at $z < 4$ is $\sim 50\%$ and therefore we do not include it in our $z \sim 6$ sample. However, the source may still correspond to a $z \sim 6$ galaxy and therefore it is worthwhile to consider.

On the basis of our own photometry, we estimate the

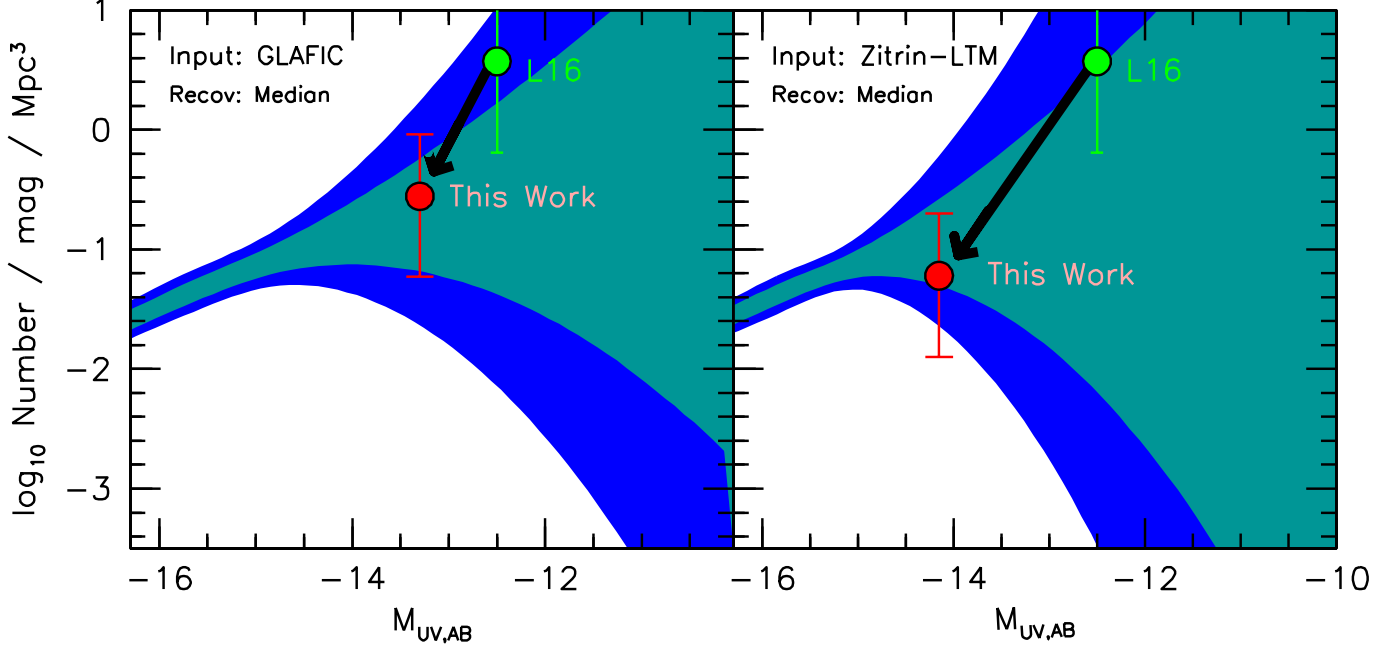


FIG. 11.— Comparison of the faintest point in the $z \sim 6$ LF from L16 (large green point with 1σ error bars) with the 68% and 95% likelihood intervals implied by our $z \sim 6$ LF results (shaded in cyan and blue, respectively) assuming that the GLAFIC and Zitrin-LTM magnification models represent reality (left and right panels, respectively). This point originates from just a single $z \sim 6$ candidate in the L16 catalog, but is important because it provides significant leverage in their discussion regarding a turn-over. While this source does not satisfy the criteria for our own $z \sim 6$ selection due to its having an estimated probability of $\sim 50\%$ of lying at $z < 4$, we can nevertheless determine the LF constraint we would obtain if we had included it in our $z \sim 6$ sample. This is shown with the large red point in each panel. The absolute magnitude we estimate for this source is 1.0 mag brighter than what L16 estimate. The Zitrin-LTM magnification model imply that this source is another factor of 3 brighter yet than in the GLAFIC models. For either lensing model, we find no significant tension between our 68% and 95% likelihood contours and the volume densities we estimate for this candidate using our own photometry and selection volume constraints. While this point plays a significant role in L16’s discussion regarding a turn-over, a reassessment of its luminosity and volume density indicates that it is consistent with other forms for the $z \sim 6$ LF, including one which shows a turn-over at ~ -15 mag.

source to have a total magnitude of 28.9 mag. Using the magnification factor of $60.6^{+129.0}_{-22.2}$ L16 estimate for the source based on current magnification models which are publicly available and a redshift of $z \sim 6$, we estimate an absolute magnitude of -13.4 mag, which is ~ 1 mag brighter than what L16 estimate for the same source.¹³ While it is unclear why our own magnitude estimates are in such large tension with those from L16, we can nevertheless examine the implications this source would have for our UV LF results if it is indeed at $z \sim 6$.

Taking this single source and dividing by the selection volume in the range $-13.5 < M_{UV,AB} < -13$, we estimate a volume density of $0.28^{+0.64}_{-0.22} \text{ Mpc}^{-3} \text{ mag}^{-1}$. Interestingly enough, this is completely consistent, as illustrated in Figure 11 (left panel), with the LF constraints we find at ~ -13.4 mag treating the GLAFIC magnification model as reality and recovering the LF results using the median magnification model. It is also consistent (right panel to Figure 11) with the LF results we derive using the other magnification models, e.g., Zitrin-LTM,

¹³ The implied apparent magnitude for the faintest source from L16 (using the quoted photometric redshift $z = 6.1$, magnification factor 60.6, and absolute magnitude measurement -12.4 for this source) is 29.9 mag, i.e., corresponding to a 2σ detection in the data. Since this is ~ 0.6 mag fainter than this source could have if the source was a reliable $>5\sigma$ detection in the observations, which would be implied by their requirement for 3.5σ detections in two WFC3/IR bands, the absolute magnitude L16 report appears to be incorrect. The correct magnitude for this source must be ~ 0.6 - 0.7 mag brighter than what L16 report, i.e., < -13.0 mag.

which suggest a magnification factor of 19 instead of the median magnification factor of ~ 60.6 found by L16 and which imply volume densities of $\sim 0.06 \text{ Mpc}^{-3} \text{ mag}^{-1}$. It is not surprising that we recover lower volume densities than recovered by L16, given our use of smaller sizes for the faint > -16 mag population as now appears to be appropriate (Bouwens et al. 2016). Smaller sizes translate into a higher estimated completeness and selection volume.

We also checked that the inclusion of this source only had a moderate impact on the allowed luminosity of a turn-over. If we include this source in the observed counts, we find our constraints on a possible turn-over in the UV LF change by 0.8 mag (becoming fainter) assuming that GLAFIC-vs.-median model are typical of the true magnification errors and by ~ 0.4 mag (becoming fainter) assuming that the Bradac-vs.-median or GRALE-vs.-median models are more typical of the errors. If we ask which luminosities we can exclude for a turn-over at 95% confidence, the excluded luminosities are < -14.7 mag for the GLAFIC-vs.-median case (2.7 mag brighter than what L16 report for this limit).

As we have seen in this section, it is not possible at present to definitively rule out the existence of a turn-over in the UV LF at ~ -15 mag and especially at ~ -14 mag on the basis of current observational data nor, in light of the new results presented in this paper, could L16 actually do so from their data.

6.3. Comparison with Theoretical Expectations

The observational constraints we have obtained here are obviously of great value for comparing against the predictions for the form of the LF at the faint end, as provided by many different teams using simulations, theoretical models, and on the basis of observations of the nearby universe.

We compare our LF constraints with the following cosmological simulation or theoretical model results:

Renaissance [O’Shea et al. 2015]: O’Shea et al. (2015) report some of the first results from the “Renaissance” simulations. The “Renaissance” simulations are zoom-in simulations of a $(28.4\text{Mpc}/h)^3$ volume of the universe, powered by the Enzo code (Bryan et al. 2014), and self-consistently following the evolution of gas and dark matter, including H_2 formation and destruction from photodissociation. Star formation and supernovae physics are included and ionizing and UV radiation are produced as predicted by Starburst99 (Leitherer et al. 1999). Individual dark-matter particles in the simulations have masses of $2.9 \times 10^4 M_\odot$, meaning that the smallest halos that are resolved in the simulation are $2 \times 10^6 M_{\text{dot}}$ (~ 70 particles/halo). Many details of the physical implementation of the implementation of the physics and also sub-grid recipes are provided in Xu et al. (2013, 2014) and Chen et al. (2014). In the “Renaissance” simulations, flattening in the UV LF is a direct result of the decreasing fraction of baryons converted to stars in the lowest mass halos, due to the impact of radiative feedback and less efficient cooling processes. While it is not yet possible to follow the results of these simulations to $z \sim 6$, results are available at $z \sim 12$ and this is the redshift we use for comparisons.

CoDa [Ocvirk et al. 2016]: The Cosmic Dawn (CoDa) simulations are full gravity + hydrodynamic simulations of a large $\sim (100\text{Mpc})^3$ volume of the universe using the RAMSES code (Teyssier 2002). The simulations include standard prescriptions for star formation and supernovae explosions following standard recipes (Ocvirk et al. 2008; Governato et al. 2009, 2010). One new feature of the CoDa simulations is the inclusion of radiative transfer into the simulations, in the sense that hydrodynamics and radiative transfer are now fully coupled. As a result, the effects of photoionization heating on low-mass galaxies are fully included in the CoDa simulations. Ocvirk et al. (2016) report that radiative feedback plays a big role in suppressing star formation in low mass galaxies and modulating the faint-end of the LF.

CROC [Gnedin 2014, 2016]: The LF results for the Cosmic Reionization On Computers (CROC) are based on gravity + hydrodynamical simulations using Adaptive Refinement Treement (ART) code (Kratsov 1999; Kravtsov 2002; Rudd et al. 2008). The CROC simulations include a wide variety of physics processes, including gas cooling and heating processes, molecular hydrogen chemistry, star formation, stellar feedback, radiative transfer of ionizing and UV light from stars. These simulations are conducted in $20h^{-1}\text{Mpc}$ boxes at a variety of resolutions. The effective slope of CROC LFs continue to flatten towards fainter magnitudes and reach a peak at ~ -12 mag. However, the peak at ~ -12 mag is reported not to be a robust prediction of the simulation and to depend on the minimum particle size in the

simulations. The impact of radiative feedback is less important in the CROC simulations than in CoDa.

Finlator et al. (2015, 2016a, 2016b): The Finlator et al. (2015, 2016a, 2016b) LF results are based on a cosmological simulation of galaxy formation in a $(7.5h^{-1})^3\text{Mpc}^3$ volume of the universe including both gravity and hydrodynamics as implemented in the GADGET-3 code (Springel 2005). To this code, gas cooling is added through collisional excitation of hydrogen and helium as in Katz et al. (1996), and metal line cooling is implemented using the collisional ionization equilibrium tables of Sutherland & Dopita (1993). Star formation is added using the Kennicutt-Schmidt law, with supernovae feedback included following the “ezw” prescription from Davé et al. (2013) and metal enrichment from supernovae as implemented as in Oppenheimer & Davé (2008). Flattening in the Finlator et al. (2015, 2016a, 2016b) LFs occurs mostly due to less efficient gas cooling at lower halo masses.

DRAGONS [Liu et al. 2016a]: The LF results from Liu et al. (2016a) are based on the Dark-ages Reionization And Galaxy-formation Observables from Numerical Simulations (DRAGONS)¹⁴ project which build semi-numerical models of galaxy formation on top of halo trees derived from N-body simulations done over different box sizes to probe a large dynamical range. The semi-numerical models include gas cooling physics, star formation prescriptions, feedback and merging prescriptions, among other components of the model. The turn-over in the LF results of Liu et al. (2016a) at ~ -12 mag correspond to the approximate halo masses $\sim 10^8 M_\odot$ where the gas temperature is 10^4K . Above this temperature, atomic cooling processes become efficient. In earlier data sets, Muñoz & Loeb (2011) had looked at what constraints could be placed on this mass using earlier LFs of Bouwens et al. (2007).

Jaacks et al. (2013): The simulation results in Jaacks et al. (2013) are powered by the GADGET-3 (Springel 2005) gravity+hydrodynamics code run in three box sizes (10, 33.75, and $100 h^{-1}\text{Mpc}$) and three different particle sizes (9×10^5 , 2×10^7 , and $3 \times 10^8 h^{-1} M_\odot$). Radiation cooling is included in the simulations by H, He, and metals (Choi & Nagamine 2009), a UV background self-shielding effect, and heating by a uniform UV background (Faucher-Giguère et al. 2009). Supernovae feedback is implemented by a momentum-drive wind model (Choi & Nagamine 2011). Star formation in the simulations is governed by SFR-vs- H_2 model of Krumholz et al. (2009) rather than in terms of the total density in cold gas. The implementation of this in the GADGET-3 code is as described in Thompson et al. (2013) and is similar to the implementation of the same recipe by Kuhlen et al. (2013) in the Enzo code. As a result of the lower gas density in molecular hydrogen H_2 in fainter, lower-mass galaxies, the LFs predicted by Jaacks et al. (2013) show a turn-over at $\sim -15.4 \pm 0.6$ mag.

Dayal et al. (2014): The LF results from Dayal et al. (2014) are based on a semi-analytic model which follows the evolution of galaxies in merger tree constructed from

¹⁴ <http://dragons.ph.unimelb.edu.au>

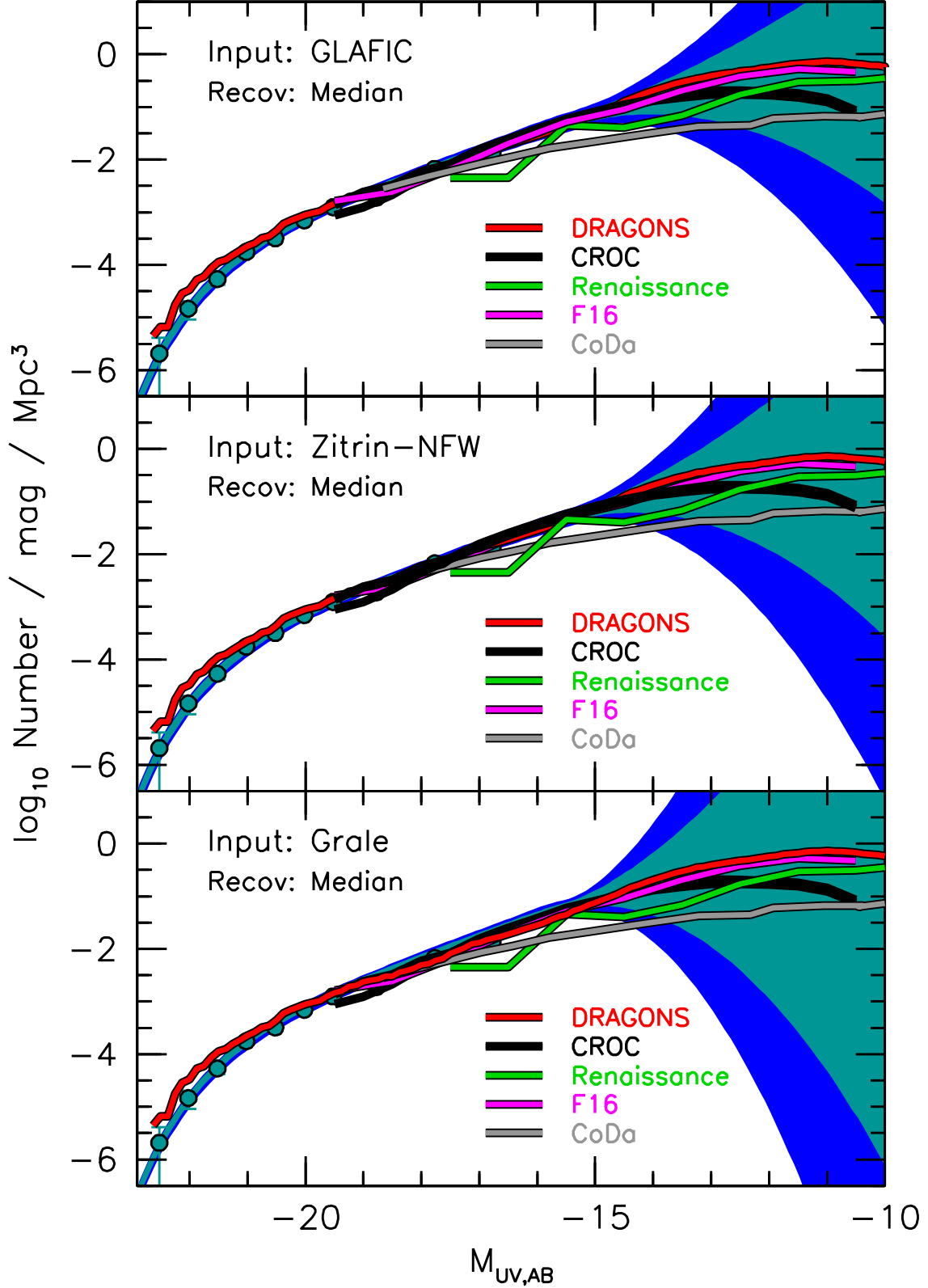


FIG. 12.— Comparison of the 68% and 95% confidence intervals we have derived on the shape of the $z \sim 6$ UV LF with the predictions for this LF. Confidence intervals are shown making different assumptions about the typical size of errors in the lensing models, assuming these errors to typically be as large as the differences between the median parametric model and the GLAFIC model, Sharon/Johnson models, and GRALE models. The plotted theoretical models include DRAGONS (red lines: Liu et al. 2016a), CROC (black lines: Gnedin 2016), ENZO (green lines: O’Shea et al. 2016), CoDa (gray lines: Ocvirk et al. 2016), and Finlator et al. (2015, 2016a, 2016b [F16]: purple lines). The LF results from O’Shea et al. (2016) rely on their $z \sim 12$ LF, since those simulations have not yet run down to $z \sim 6$. Overall, we find good agreement between the predicted LF results and the present observational constraints.

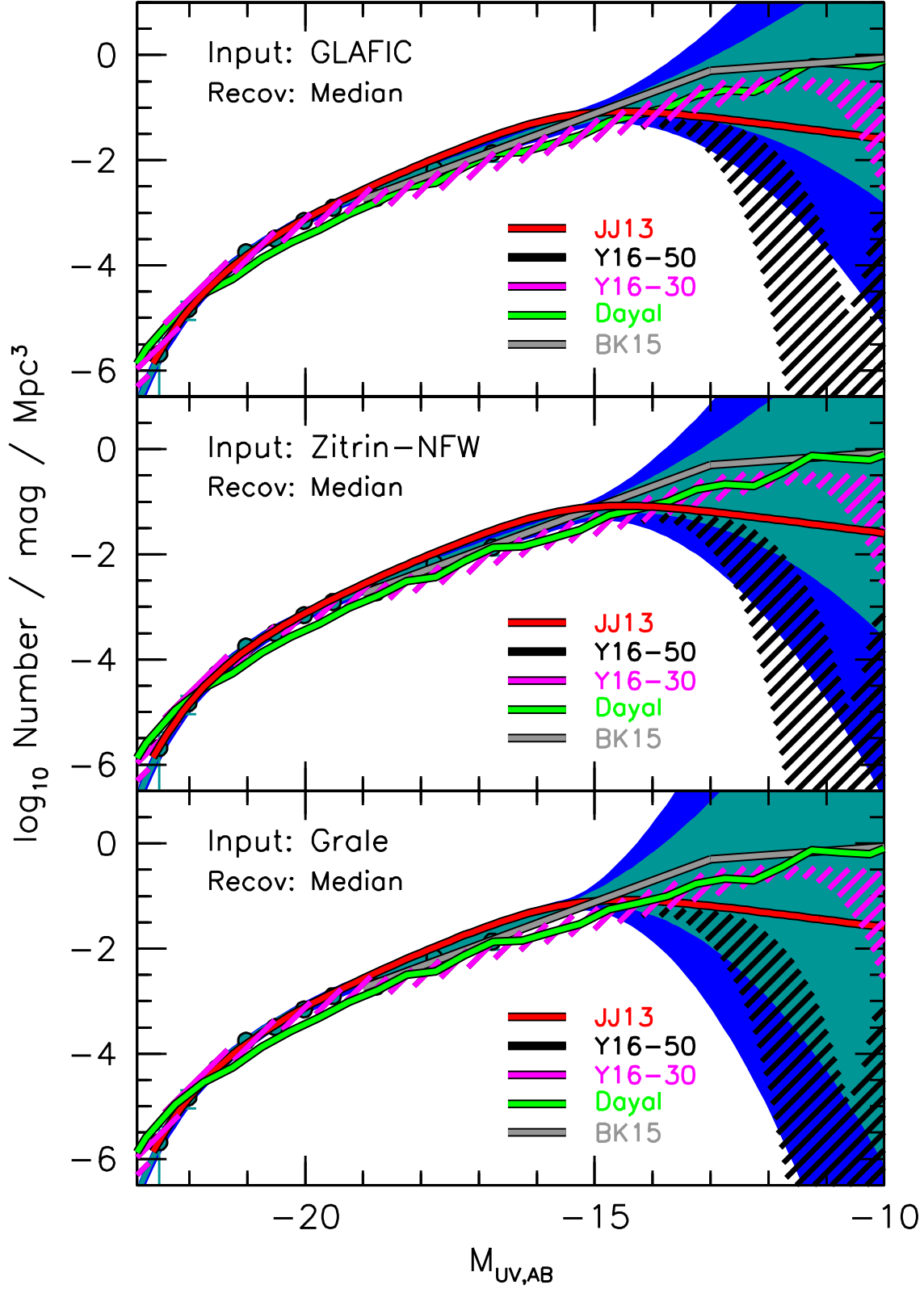


FIG. 13.— Identical to Figure 12 but showing the results for the Jaacks et al. (2013: JJ13) model, two different models from Yue et al. (2016) where radiative feedback becomes important at circular velocities of 30 km s⁻¹ and 50 km s⁻¹, and the Dayal et al. (2014) model. The dip at -11 mag in the 50 km s⁻¹ Yue et al. (2016) model is due to the quenching of star formation in low-mass halos from radiative feedback. Also included among the presented results are the LF constraints implied from the abundance matching analysis Boylan-Kolchin et al. (2015: BK15) perform using dwarfs in the nearby universe.

extended Press-Schechter theory (Lacey & Cole 1993). The star formation rate in individual proceed at such a rate as to balance the impact of supernovae feedback in expelling all the gas from a galaxy. Flattening in the UV LF is partially the result of a similar flattening in the halo mass function, as well as lower efficiency for star formation in the lower-mass halos that contribute to the low luminosity end of the LF.

Yue et al. (2016): Yue et al. (2016) derive their LF results assuming a non-evolving stellar mass-halo mass relation. Yue et al. (2016) adopt a very similar approach to what Mason et al. (2015) employ in predicting the galaxy LF (see also Trenti et al. 2010 and Tacchella et al. 2013). Yue et al. (2016) start with the halo mass function, break up the star formation history of each halo into segments according to which the halo grows in mass by a factor of two, and then assume that the SFR must be such to maintain a constant stellar mass-halo mass relation which they calibrate to the $z \sim 5$ LF of Bouwens et al. (2016). Yue et al. (2016) then look into the impact that radiative feedback could have during the epoch of reionization. Yue et al. (2016) derive their LF results assuming that halos below some fixed circular velocity would have their star formation quenched.

Finally, we also include a comparison with the empirical results on the faint end of the LF at high redshift:

Boylan-Kolchin et al. (2015): Boylan-Kolchin et al. (2015) arrive at constraints on the faint-end of the LF at $z \sim 7$ by leveraging deep probes of the color-magnitude relationship of nearby dwarf galaxies which allow one to estimate the luminosity of these sources at $z \sim 7$. By comparing the distribution of inferred luminosities of these dwarfs with the expected numbers extrapolating $z \sim 7$ LFs to -10 mag, Boylan-Kolchin et al. (2015) infer a break in the LF at ~ -13 mag from a faint-end slope of ~ -2 to ~ -1.2 .

We present comparisons of the predicted LFs from both sophisticated hydrodynamical simulations, various semi-analytic models, and the empirical results of Boylan-Kolchin et al. (2015) in Figures 12 and 13.

Overall, we find reasonable agreement between our observational results and the predicted LFs from both hydrodynamic simulations and various semi-empirical theoretical models. The predicted LFs from the CoDa simulation (Ocvirk et al. 2016) and from two semi-analytical models Yue et al. (2016) and Dayal et al. (2016) against which we compare fall slightly below our observational constraints at -15.5 mag by ~ 0.2 - 0.3 dex, but otherwise are in reasonable agreement with our results.

In particular, we find that our observational constraints allow for the existence of a flattening or turn-over in the $z \sim 6$ LF at > -15 mag as predicted in the theoretical models, due to a variety of physical processes, including a greater role for radiative feedback (O’Shea et al. 2015; Ocvirk et al. 2016; Yue et al. 2016) and less efficient cooling in lower mass halos where atomic cooling processes would be less important (Wise et al. 2014; Gnedin 2016; Liu et al. 2016a). The present results suggest that these physical processes can impact the shape of the LF at > -15 mag, as is predicted, and there is no fundamental disagreement with observational results to > -14 mag (contrary to reports from L16).

Our observational results are also fully consistent with the abundance matching constraints obtained by Boylan-Kolchin et al. (2015) which suggest a break in the faint end slope of the LF at -13 mag. The toy LF from Boylan-Kolchin et al. (2015) is almost entirely contained within our 68% confidence intervals, suggesting that the flattening they infer from analyses of nearby dwarf galaxies is fully consistent with the HFF observations of faint $z \sim 6$ galaxies.

7. SUMMARY

Here we have made use of a large selection of 160 lensed $z \sim 6$ galaxies from the first four HFF clusters to constrain the shape of the $z \sim 6$ UV LF to very low luminosities. Not only does the present sample of lensed $z \sim 6$ galaxies represent the most comprehensive such sample to date, but the present sample probes to equivalently low luminosities as other work (if we account for the fact that others report luminosities up to 0.7 - 1.0 mag fainter than what we find for the same sources [though ~ 0.5 mag is more typical]: see §2 and §6.1-§6.2). Our analysis provides a much more realistic assessment of the impact of the large magnification uncertainties inherent at high magnifications. This allows us to set improved constraints on the faint-end slope α and also to investigate whether the UV LF shows a turn-over at very low luminosities.

One particular emphasis of this analysis was to include a full account of systematic errors in deriving accurate constraints on the shape of the $z \sim 6$ UV LF. We looked especially at the impact of errors in the magnification maps, but we also considered the impact of uncertainties in the estimated completeness based on the size distribution building upon results in a companion paper (Bouwens et al. 2016).

To explore the impact of errors in the magnification map on LF results, we have developed a new forward modeling approach which involves using one set of magnification models and a candidate LF to create mock catalogs over each of the HFF clusters. These catalogs are then analyzed using the same type of magnification models as are used to interpret the real observations (Figure 5). The likelihood of a given LF can then be assessed by comparing the observed counts with the expected counts derived from the simulations. Our quantification of the general form of the $z \sim 6$ LF includes not only the normal Schechter parameters, but also a curvature parameter δ which we apply faintward of -16 mag to characterize the form of the LF to very low luminosities.

Our new simulation results using forward modeling demonstrate the basic impact of magnification errors on the LF results. We show that scatter due to magnification errors results in the LF showing a faint-end slope of ~ -2 or steeper in the very low luminosity regime where the magnification factors are high $\mu > 10$ - 30 . This effect is so pervasive that it can eliminate any indication of a turn-over (even if present in reality) at the faint end of the LF (see Figure 4). At lower magnification factors, i.e., $\mu < 10$, where the predictive power of the magnification models is best (e.g., see Figure 3 and also Meneghetti et al. 2016), the impact appears to be most manageable in terms of the overall impact on the LF results.

For higher magnification factors, i.e., at $\mu > 10$ and

especially at $\mu > 30$, the predictive power of the magnification models is much poorer, resulting in large uncertainties in the magnification factors. As a result, it can be difficult to determine whether the LF shows a turn-over at ~ -15 mag, whether it steepens further at ~ -15 mag, or whether it continues with a fixed faint-end slope to -12 mag (see Figure 4).

Taking advantage of our forward modeling procedure, we derive new constraints on the faint-end slope of the LF and arrive at a value of -1.92 ± 0.04 using the HFF observations alone (Table 2) and -1.92 ± 0.04 combining our constraints with the field results of Bouwens et al. (2015). Both constraints are consistent with our previous determination $\alpha = -1.87 \pm 0.10$ (Bouwens et al. 2015) using the HUDF+HUDF-parallel+CANDELS data alone. We nevertheless caution that the faint-end slope could be up to $\Delta\alpha \sim 0.15$ steeper if our search for faint $z \sim 6$ galaxies is $2\times$ more incomplete than we assume. This is a direct result of the unknown size distribution of extremely faint galaxies.

We use our new constraints to derive 68% and 95% confidence regions on the faint-end form of the $z \sim 6$ LF, presenting our results in Figure 7. We find no evidence for a turn-over in the LF at the faint end. Nevertheless, we can place constraints on how faint it must be, though the result does depend on the assumed size of the errors in the magnification models. If the true errors in the models are similar to the differences between the GLAFIC model and the median parametric model, our results strongly indicate that a turn-over cannot occur brightward of -14.2 mag (68% confidence). However, if differences between the non-parametric models and the median parametric models are typical, then a turn-over cannot occur brightward of -15.3 mag (68% confidence). Our results are fully consistent with recent observational results from Boylan-Kolchin et al. (2015) and theoretical models (O’Shea et al. 2015; Gnedin 2016; Liu et al. 2016a; Ocvirk et al. 2016) predicting some flattening in the UV LFs at > -15 mag.

The faint-end slope α we derive at $z \sim 6$ is -1.92 ± 0.04 and 3.5σ shallower than the L16 faint-end slope $\alpha = -2.10 \pm 0.03$ (statistical error only). Meanwhile, our

constraints on the turn-over are consistent with the findings by Atek et al. (2015) and Castellano et al. (2016b), but are weaker than what L16 report. Despite having larger samples than L16 and considering twice as many HFF clusters (while probing to comparably low luminosities), we only find evidence against a turn-over brightward of ~ -15.3 and ~ -14.2 mag at 68% confidence, vs. the ~ -11.1 mag reported by L16 at nominally slightly higher confidence. We speculate that L16’s stronger claims against a turn-over (and steeper faint-end slope results) arose as a result of artifacts in their determinations of the LFs resulting from likely inaccurate size assumptions (see §6.1-6.2 and Bouwens et al. 2016) and also a possible bias in their measurements of the total luminosities of sources (§6.1.2).

The new formalism we have developed to derive LF results in the presence of errors in the magnification map has significant utility and can be applied to other *HST* observations that have been obtained with the HFF program. In the immediate future, we plan to make use of our new forward-modeling methodology to derive LF results at $z \sim 6$, $z \sim 7$, $z \sim 8$, and $z \sim 9$ from the full HFF program. These results would provide us perhaps our most complete information on the faint-end form of the LFs before JWST and provide us with clues as to how the overall ionizing emissivity evolves with cosmic time.

We acknowledge many useful conversations on the algorithms presented in this paper with Marijn Franx. We are greatly appreciative to Pratika Dayal, Kristian Finlator, Nicholas Gnedin, Chuanwu Liu, Brian O’Shea, Pierre Ocvirk, and Bin Yue for sending us the predictions they derive for the LF results at high redshift. We thank Kristian Finlator for discussing with us at length different turn-over mechanisms that would impact the UV LF at low luminosities. Austin Hoag kindly sent us the v2 Bradac models for HFF cluster MACS0416. RSE acknowledges financial support from the European Research Council under Advanced Grant FP7/669253.

REFERENCES

- Alavi, A., Siana, B., Richard, J., et al. 2014, *ApJ*, 780, 143
 Alavi, A., Siana, B., Richard, J., et al. 2016, *ApJ*, in press, arXiv:1606.00469
 Atek, H., Richard, J., Kneib, J.-P., et al. 2014, *ApJ*, 786, 60
 Atek, H., Richard, J., Kneib, J.-P., et al. 2015a, *ApJ*, 800, 18
 Atek, H., Richard, J., Jauzac, M., et al. 2015b, *ApJ*, 814, 69
 Beckwith, S. V. W., Stiavelli, M., Koekemoer, A. M., et al. 2006, *AJ*, 132, 1729
 Bertin, E. and Arnouts, S. 1996, *A&AS*, 117, 39
 Bouwens, R. J., Illingworth, G. D., Franx, M., & Ford, H. 2007, *ApJ*, 670, 928
 Bouwens, R. J., Illingworth, G. D., Oesch, P. A., et al. 2012, *ApJ*, 754, 83
 Bouwens, R., Bradley, L., Zitrin, A., et al. 2014b, *ApJ*, 795, 126
 Bouwens, R. J., Illingworth, G. D., Oesch, P. A., et al. 2015, *ApJ*, 803, 34
 Bouwens, R. J., Illingworth, G. D., Oesch, P. A., et al. 2015, *ApJ*, 811, 140
 Bouwens, R. 2016, Understanding the Epoch of Cosmic Reionization: Challenges and Progress, 423, 111
 Bouwens, R. J., Illingworth, G. D., Oesch, P. A., et al. 2016, *ApJ*, submitted, arXiv:1608.00966
 Bowler, R. A. A., Dunlop, J. S., McLure, R. J., et al. 2015, *MNRAS*, 452, 1817
 Boylan-Kolchin, M., Bullock, J. S., & Garrison-Kimmel, S. 2014, *MNRAS*, 443, L44
 Boylan-Kolchin, M., Weisz, D. R., Johnson, B. D., et al. 2015, *MNRAS*, 453, 1503
 Dunlop, J. S., McLure, R. J., et al. 2015, *MNRAS*, 452, 1817
 Bradač, M., Treu, T., Applegate, D., et al. 2009, *ApJ*, 706, 1201
 Bryan, G. L., Norman, M. L., O’Shea, B. W., et al. 2014, *ApJS*, 211, 19
 Castellano, M., Amorín, R., Merlin, E., et al. 2016a, *A&A*, 590, A31
 Castellano, M., Yue, B., Ferrara, A., et al. 2016b, *ApJ*, 823, L40
 Chen, P., Wise, J. H., Norman, M. L., Xu, H., & O’Shea, B. W. 2014, *ApJ*, 795, 144
 Choi, J.-H., & Nagamine, K. 2009, *MNRAS*, 393, 1595
 Choi, J.-H., & Nagamine, K. 2011, *MNRAS*, 410, 2579
 Coe, D., Bradley, L., & Zitrin, A. 2015, *ApJ*, 800, 84
 Davé, R., Katz, N., Oppenheimer, B. D., Kollmeier, J. A., & Weinberg, D. H. 2013, *MNRAS*, 434, 2645
 Dayal, P., Ferrara, A., Dunlop, J. S., & Pacucci, F. 2014, *MNRAS*, 445, 2545

- Diego, J. M., Broadhurst, T., Molnar, S. M., Lam, D., & Lim, J. 2015, *MNRAS*, 447, 3130
- Duncan, K., & Conselice, C. J. 2015, *MNRAS*, 451, 2030
- Dunlop, J. S., Rogers, A. B., McLure, R. J., et al. 2013, *MNRAS*, 432, 3520
- Ellis, R. S., McLure, R. J., Dunlop, J. S., et al. 2013, *ApJ*, 763, L7
- Faucher-Giguère, C.-A., Lidz, A., Zaldarriaga, M., & Hernquist, L. 2009, *ApJ*, 703, 1416
- Finkelstein, S. L., Papovich, C., Salmon, B., et al. 2012, *ApJ*, 756, 164
- Finkelstein, S. L., Ryan, R. E., Jr., Papovich, C., et al. 2014, *ArXiv e-prints*
- Finlator, K., Thompson, R., Huang, S., et al. 2015, *MNRAS*, 447, 2526
- Finlator, K., Oppenheimer, B. D., Davé, R., et al. 2016a, *MNRAS*, 459, 2299
- Finlator, K., Prescott, M. K. M., Oppenheimer, B. D., et al. 2016b, *MNRAS*, in press, arXiv:1609.06348
- Giallongo, E., Grazian, A., Fiore, F., et al. 2015, *A&A*, 578, A83
- Gnedin, N. Y. 2014, *ApJ*, 793, 29
- Gnedin, N. Y. 2016, *ApJ*, 825, L17
- Grazian, A., Castellano, M., Koekemoer, A. M., et al. 2011, *A&A*, 532, A33
- Grogin, N. A., Kocevski, D. D., Faber, S. M., et al. 2011, *ApJS*, 197, 35
- Illingworth, G. D., Magee, D., Oesch, P. A., et al. 2013, *ApJS*, 209, 6
- Ishigaki, M., Kawamata, R., Ouchi, M., et al. 2015, *ApJ*, 799, 12
- Jaacks, J., Thompson, R., & Nagamine, K. 2013, *ApJ*, 766, 94
- Jauzac, M., Jullo, E., Eckert, D., et al. 2015a, *MNRAS*, 446, 4132
- Jauzac, M., Richard, J., Jullo, E., et al. 2015b, *MNRAS*, 452, 1437
- Johnson, T. L., Sharon, K., Bayliss, M. B., et al. 2014, *ApJ*, 797, 48
- Jullo, E., & Kneib, J.-P. 2009, *MNRAS*, 395, 1319
- Katz, N., Weinberg, D. H., & Hernquist, L. 1996, *ApJS*, 105, 19
- Kawamata, R., Ishigaki, M., Shimasaku, K., Oguri, M., & Ouchi, M. 2015, *ApJ*, 804, 103
- Kawamata, R., Oguri, M., Ishigaki, M., Shimasaku, K., & Ouchi, M. 2016, *ApJ*, 819, 114
- Koekemoer, A. M., Faber, S. M., Ferguson, H. C., et al. 2011, *ApJS*, 197, 36
- Kravtsov, A. V. 1999, Ph.D. Thesis, 5564
- Kravtsov, A. V., Klypin, A., & Hoffman, Y. 2002, *ApJ*, 571, 563
- Kravtsov, A. V. 2013, *ApJ*, 764, L31
- Kron, R. G. 1980, *ApJS*, 43, 305
- Krumholz, M. R., McKee, C. F., & Tumlinson, J. 2009, *ApJ*, 699, 850
- Krumholz, M. R., & Dekel, A. 2012, *ApJ*, 753, 16
- Kuhlen, M., & Faucher-Giguère, C.-A. 2012, *MNRAS*, 423, 862
- Kuhlen, M., Madau, P., & Krumholz, M. R. 2013, *ApJ*, 776, 34
- Lacey, C., & Cole, S. 1993, *MNRAS*, 262, 627
- Laporte, N., Infante, L., Troncoso Iribarren, P., et al. 2016, *ApJ*, 820, 98
- Leitherer, C., Schaerer, D., Goldader, J. D., et al. 1999, *ApJS*, 123, 3
- Liesenborgs, J., De Rijcke, S., & Dejonghe, H. 2006, *MNRAS*, 367, 1209
- Liu, C., Mutch, S. J., Angel, P. W., et al. 2016a, *MNRAS*, 462, 235
- Liu, C., Mutch, S., Poole, G., et al. 2016b, arXiv:1608.00819
- Livermore, R., Finkelstein, S., Lotz, J. 2016, *ApJ*, submitted, arXiv:1604.06799
- Lotz, J. M., Koekemoer, A., Coe, D., et al. 2016, arXiv:1605.06567
- Madau, P., & Haardt, F. 2015, *ApJ*, 813, L8
- Maizy, A., Richard, J., de Leo, M. A., Pelló, R., & Kneib, J. P. 2010, *A&A*, 509, A105
- Mason, C. A., Trenti, M., & Treu, T. 2015, *ApJ*, 813, 21
- McGreer, I. D., Jiang, L., Fan, X., et al. 2013, *ApJ*, 768, 105
- McLure, R. J., Dunlop, J. S., Bowler, R. A. A., et al. 2013, *MNRAS*, 432, 2696
- Meneghetti, M., Natarajan, P., Coe, D., et al. 2016, arXiv:1606.04548
- Merlin, E., Amorín, R., Castellano, M., et al. 2016, *A&A*, 590, A30
- Merten, J., Meneghetti, M., Postman, M., et al. 2015, *ApJ*, 806, 4 [Mitra et al.(2015)]2015MNRAS.454L..76M Mitra, S., Choudhury, T. R., & Ferrara, A. 2015, *MNRAS*, 454, L76
- Mitra, S., Choudhury, T. R., & Ferrara, A. 2016, arXiv:1606.02719
- Muñoz, J. A., & Loeb, A. 2011, *ApJ*, 729, 99
- Navarro, J. F., Frenk, C. S., & White, S. D. M. 1997, *ApJ*, 490, 493
- Nestor, D. B., Shapley, A. E., Kornei, K. A., Steidel, C. C., & Siana, B. 2013, *ApJ*, 765, 47
- Ocvirk, P., Gillet, N., Shapiro, P. R., et al. 2015, in press, arXiv:1511.00011
- Oesch, P. A., Bouwens, R. J., Illingworth, G. D., et al. 2015, *ApJ*, 808, 104
- Oguri, M. 2010, *PASJ*, 62, 1017
- Oppenheimer, B. D., & Davé, R. 2008, *MNRAS*, 387, 577
- O'Shea, B. W., Wise, J. H., Xu, H., & Norman, M. L. 2015, *ApJ*, 807, L12
- Parsa, S., Dunlop, J. S., McLure, R. J., & Mortlock, A. 2016, *MNRAS*, 456, 3194
- Peng, C. Y., Ho, L. C., Impey, C. D., & Rix, H.-W. 2002, *AJ*, 124, 266
- Planck Collaboration, Ade, P. A. R., Aghanim, N., et al. 2015, arXiv:1502.01589 [PC15]
- Priewe, J., Williams, L. L. R., Liesenborgs, J., Coe, D., & Rodney, S. A. 2016, *MNRAS*, submitted, arXiv:1605.07621
- Richard, J., Jauzac, M., Limousin, M., et al. 2014, *MNRAS*, 444, 268
- Robertson, B. E., Furlanetto, S. R., Schneider, E., et al. 2013, *ApJ*, 768, 71
- Robertson, B. E., Ellis, R. S., Dunlop, J. S., et al. 2014, *ApJ*, 796, L27
- Robertson, B. E., Ellis, R. S., Furlanetto, S. R., & Dunlop, J. S. 2015, *ApJ*, 802, L19
- Rodney, S. A., Patel, B., Scolnic, D., et al. 2015, *ApJ*, 811, 70
- Rogers, A. B., McLure, R. J., Dunlop, J. S., et al. 2014, *MNRAS*, 440, 3714
- Rudd, D. H., Zentner, A. R., & Kravtsov, A. V. 2008, *ApJ*, 672, 19
- Schenker, M. A., Robertson, B. E., Ellis, R. S., et al. 2013, *ApJ*, 768, 196
- Schwarz, G., 1978, *The annals of statistics*, 6, 461
- Sebesta, K., Williams, L. L. R., Mohammed, I., Saha, P., & Liesenborgs, J. 2016, *MNRAS*, 461, 2126
- Shibuya, T., Ouchi, M., & Harikane, Y. 2015, *ApJS*, 219, 15
- Siana, B., Teplitz, H. I., Ferguson, H. C., et al. 2010, *ApJ*, 723, 241
- Siana, B. 2013, *HST Proposal*, 13389
- Siana, B. 2015, *HST Proposal*, 14209
- Siana, B., Shapley, A. E., Kulas, K. R., et al. 2015, *ApJ*, 804, 17
- Skelton, R. E., Whitaker, K. E., Momcheva, I. G., et al. 2014, *ApJS*, 214, 24
- Somerville, R. S., Lee, K., Ferguson, H. C., et al. 2004, *ApJ*, 600, L171
- Springel, V. 2005, *MNRAS*, 364, 1105
- Sutherland, R. S., & Dopita, M. A. 1993, *ApJS*, 88, 253
- Tacchella, S., Trenti, M., & Carollo, C. M. 2013, *ApJ*, 768, L37
- Teyssier, R. 2002, *A&A*, 385, 337
- Thompson, R., Nagamine, K., Jaacks, J., & Choi, J.-H. 2014, *ApJ*, 780, 145
- Trenti, M., & Stiavelli, M. 2008, *ApJ*, 676, 767
- Trenti, M., Stiavelli, M., Bouwens, R. J., et al. 2010, *ApJ*, 714, L202
- Vanzella, E., Guo, Y., Giallisco, M., et al. 2012, *ApJ*, 751, 70
- Vanzella, E., de Barros, S., Vasei, K., et al. 2016, *ApJ*, 825, 41
- Wilkins, S. M., Bunker, A. J., Stanway, E., Lorenzoni, S., & Caruana, J. 2011, *MNRAS*, 417, 717
- Wise, J. H., Demchenko, V. G., Halicek, M. T., et al. 2014, *MNRAS*, 442, 2560
- Xu, H., Wise, J. H., & Norman, M. L. 2013, *ApJ*, 773, 83
- Xu, H., Ahn, K., Wise, J. H., Norman, M. L., & O'Shea, B. W. 2014, *ApJ*, 791, 110
- Yue, B., Ferrara, A., & Xu, Y. 2016, arXiv:1604.01314
- Zitrin, A., Broadhurst, T., Bartelmann, M., et al. 2012, *MNRAS*, 423, 2308
- Zitrin, A., Meneghetti, M., Umetsu, K., et al. 2013, *ApJ*, 762, L30
- Zitrin, A., Fabris, A., Merten, J., et al. 2015, *ApJ*, 801, 44

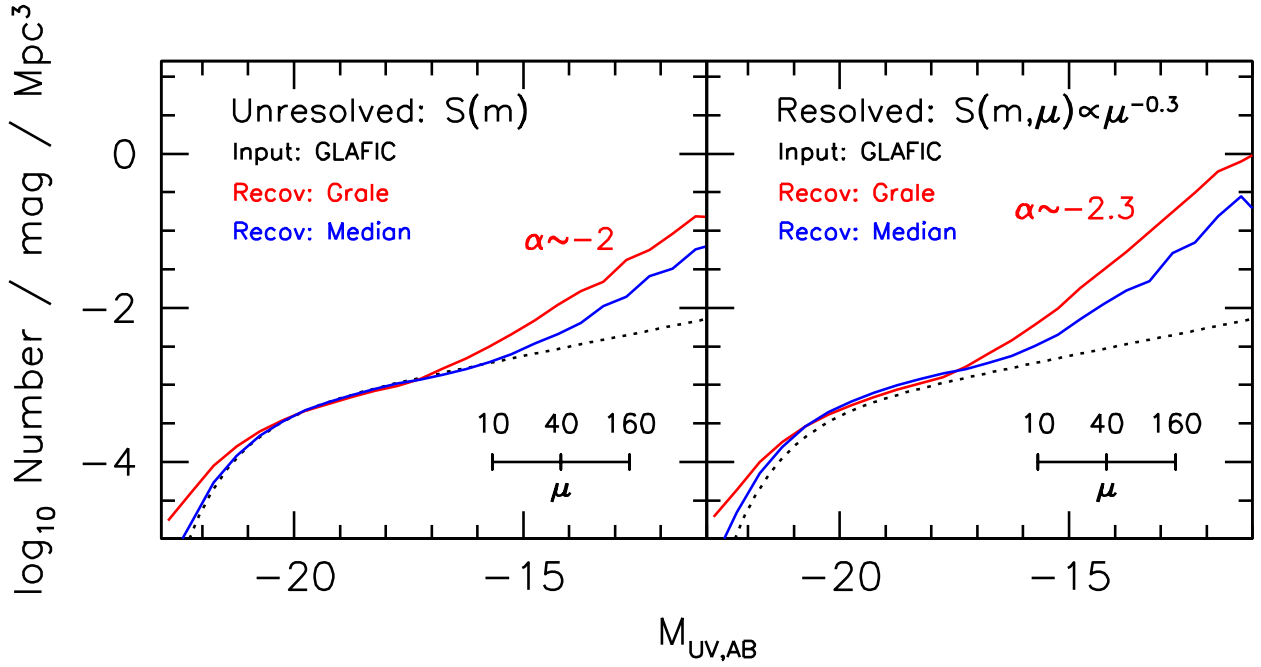


FIG. 14.— Illustration of how the impact of magnification errors on the recovered LFs depends on the sizes of sources (Appendix B). The magnification scale in the corner is as in Figure 4. An input LF with a faint-end slope of -1.3 and no turn-over at the faint end is assumed. In our forward modeling procedure, the GLAFIC magnification model is used to create the mock catalogs, while the GRALE and median magnification maps are used for recovering the LFs (red and blue lines, respectively). The left panel shows the recovered LFs assuming that point-source spatial profiles for all galaxies, while the right panel shows the recovered LFs assuming more extended sources and where the selection efficiency $S(\mu)$ decreases towards large magnification factors as $\mu^{-0.3}$ (as in Figure 3 from Oesch et al. 2015). The recovered LFs shows a departure from the input LF at ~ -15.5 mag, asymptoting towards a slope of -2 for unresolved sources (left panel) and -2.3 for resolved sources (right panel). Previous studies appear to have completely ignored the issue raised in this figure.

APPENDIX

A. SELECTION VOLUME ESTIMATES

Here we describe our procedure for estimating the effective selection volumes for faint galaxies behind the HFF clusters we examine.

Our baseline treatment is to model faint galaxies as point sources in estimating their selection volumes. This choice is motivated by our demonstration in Bouwens et al. (2016) that the faintest $z \sim 2-8$ galaxies behind the HFF clusters appeared consistent with having essentially point-source spatial profiles, with no discernible extension along the expected shear axes. Also, no discernible dependence was found for the measured surface densities as a function of the predicted shear in the high-magnification regions. Nonetheless, as such small sizes for galaxies are unexpected (e.g., Liu et al. 2016b; Kratsov 2013), we also consider the impact of larger sizes (and a larger incompleteness) on the LF results throughout the paper.

As point sources, the only quantity of importance from the lensing model is the magnification factor; the form of the deflection (or shear) map has no impact on the results. This simplifies the selection volume simulations enormously, since it means we can estimate the selection volumes for extremely faint sources in the presence of lensing in exactly the same way we would estimate the selection volumes in the absence of lensing. The only quantity of importance in estimating the selection volumes is the apparent magnitudes of the sources. Bouwens et al. (2016) discuss this in their §6.3.

We adopt a median value of -2.2 for the UV -continuum slope for galaxies in our simulations to match that found in the observations (e.g., Bouwens et al. 2014; see also Wilkins et al. 2011; Bouwens et al. 2012; Finkelstein et al. 2012; Dunlop et al. 2013; Rogers et al. 2014; Duncan & Conselice 2015).

Adopting these assumptions for the color of the sources and a point-source assumption for the size, we create artificial images for each source over the full suite of passbands and insert these images into the real observations. We then do object detection and photometry using the same procedure as we use in constructing our catalogs (§3) and then apply our selection criteria. In this way, we derive the completeness for sources in different regimes.

Selection volumes are computed by multiplying the cosmological volume element by the estimated completeness and integrating over redshift.

B. SOURCE SIZE MODULATES THE IMPACT MAGNIFICATION ERRORS HAVE ON THE INFERRED SHAPE OF THE LF

The impact of magnification errors on the derived LF can also depend on source size, as discussed in §4.1. This can occur as a result of the fact that higher magnification sources are more generally more difficult to detect, if they are

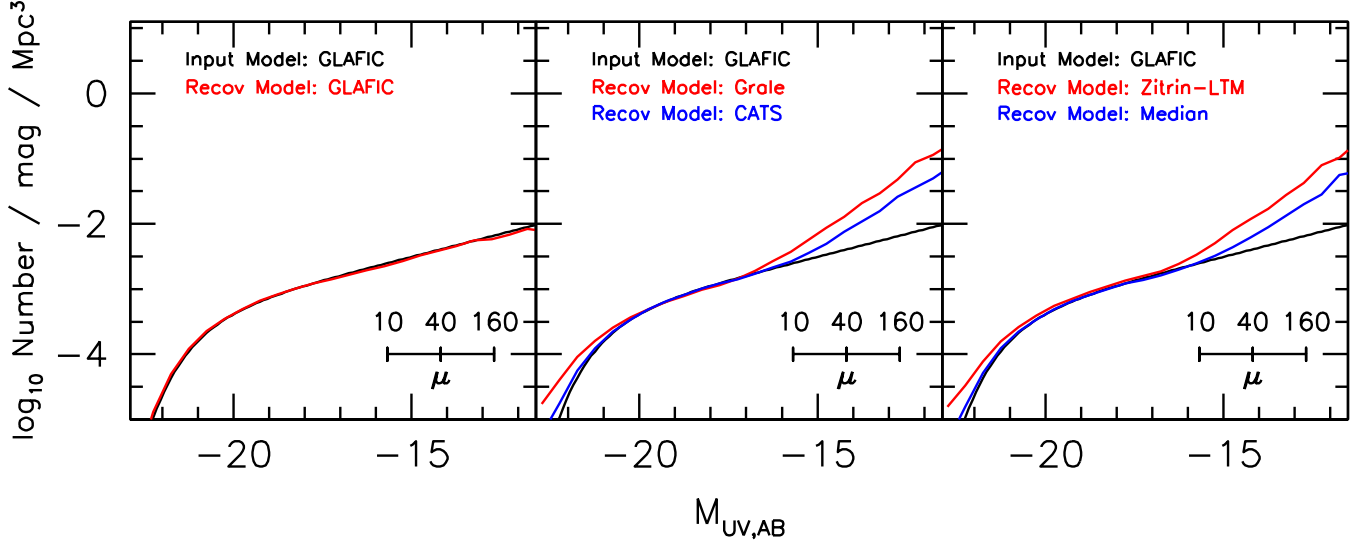


FIG. 15.— Comparison of an input LF with a shallower faint-end slope of -1.3 with the recovered LFs using a forward-modeling procedure where we create mock catalogs using the GLAFIC magnification maps and recover the LF results using the CATS, GRALE, Zitrin-LTM, and median parametric magnification maps (see Appendix C). The typical magnification levels of sources probing a given luminosity range are indicated by magnification scale in the corner. The recovered LFs show excellent agreement with the input LFs to -16.5 mag, but show a departure at -15 mag and rapidly asymptote towards a faint-end slope of -2 . Interestingly, the absolute magnitudes M_{UV} where this departure occurs correspond to magnification factors where the models lose their predictive power (Figure 3).

spatially extended, than if their magnification is lower. In other words, the selection efficiency S is a function of the magnification factor μ .

The issue is that while the actual surface density of sources in our catalogs is proportional to $S(\mu_{true})$, the selection volumes we estimate for these sources is $S(\mu_{model})$. This results in the recovered volume density for these sources being higher than the true surface density by the factor $\langle S(\mu_{true}) \rangle / \langle S(\mu_{model}) \rangle$. When $\langle \mu_{true} \rangle \sim \langle \mu_{model} \rangle$, no bias is present in the recovery volume density of sources. However, when $\langle \mu_{true} \rangle$ is less than $\langle \mu_{model} \rangle$, as is often the case at higher magnifications $\mu > 10$ (Figure 3), the recovered surface density of sources can be significantly higher than reality. For example, assuming that $S(\mu) \propto \mu^{-0.3}$ as in Figure 3 of Oesch et al. (2015), the LF asymptotes towards a faint-end slope of -2.3 .

To illustrate the impact of source size and different assumptions about $S(\mu)$, we consider two different cases: the first involving point sources where S is independent of μ and the second involving extended sources where $S(\mu)$ is proportional to $\mu^{-0.3}$. Similar to the simulations run in §3.2, we use the GLAFIC model to construct mock catalogs and then recover the LF using either the GRALE model (red line) or the median parametric magnification model (blue line). In the two cases, we incorporate the different dependencies of S on the magnification factor μ for both the catalog construction and recovery of the LF. The input LF for the simulations has a faint-end slope of -1.3 , with no turn-over at the faint end.

The results are presented in Figure 14, and the differences between the two size cases are immediately obvious. In the point source case, the faint-end slope asymptotes to -2 . However, in the case of extended sources, the faint-end slope instead asymptotes to -2.3 . In either case, the LFs asymptotically approach these slopes faintward of -16 mag assuming the GRALE model and faintward of -15 assuming the median parametric magnification model.

This example should reinforce how difficult it is to obtain accurate constraints on the shape of the LF at > -15 mag and thus to detect the existence of a flattening or turn-over in the LF. Not only do the results depend on the magnification level to which magnification maps retain their predictive power (e.g., see Figure 3), but the results also depend significantly (i.e., $\Delta\alpha \sim 0.3$) on the size distribution for faint sources.

We emphasize that the impact this has on the LF shape is distinct from the effect already discussed in the companion study to the present one (Bouwens et al. 2016), where the faint-end slope α of the LF could be biased if the sizes and hence selection volumes were improperly estimated. This bias explicitly arises *because of errors in the magnification map* and due to mismatches between $\langle S(\mu_{true}) \rangle$ and $\langle S(\mu_{model}) \rangle$.

If faint sources are slightly resolved (after magnification) – as assumed in many recent studies of faint galaxies – this bias has the potential to be quite significant at absolute magnitudes M_{UV} of > -15 mag where $\mu > 20$. Amazingly, however, previous work appear to have neither recognized the importance of such a bias, not made use of procedures that would allow for its correction, even though given the size assumptions in e.g. L16, this bias would constitute an important effect.

C. RECOVERY OF LFS WITH SHALLOWER FAINT-END SLOPES

Errors in the magnification maps can have a substantial impact on the shape of the $z \sim 6$ LF faintward of -15 mag. We already illustrated this in §3.2 of this paper using a LF which turned over at -15 mag (Figure 4).

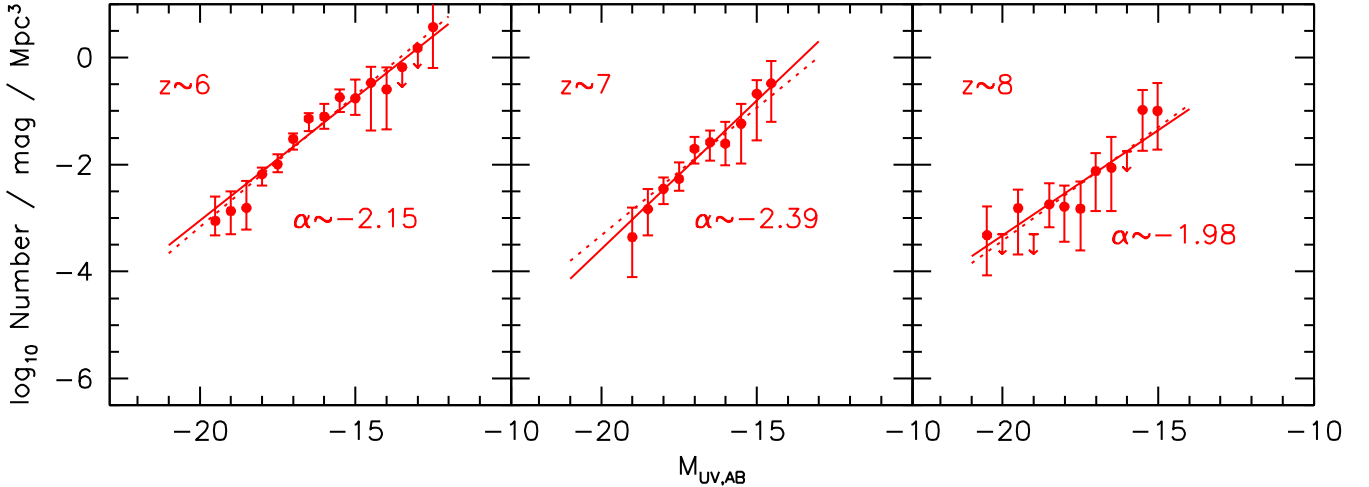


FIG. 16.— Power-law fits (*solid lines*) to the binned $z \sim 6, 7$, and 8 LF results from L16 in an effort to estimate the faint-end slope estimates from the HFF results alone. Also presented (*dotted lines*) are fits done to the L16 HFF LF results anchored to the field LF results from the same group (Finkelstein et al. 2015) at $M_{UV,AB} = -20$. The motivation for deriving the faint-end slopes α from the HFF results alone is to keep the derived results independent of those derived for the field. This makes it possible to compare the lensed LF results and field LF results in a fair way, as we do in Figure 1.

Here we show the impact of these magnification errors using a $z \sim 6$ LF with a faint-end slope -1.3 , which we intentionally take to be substantially shallower than -2 (the direction in which magnification errors drive the apparent faint-end slope). Again, we use a forward modeling procedure where we create the mock catalogs using the GLAFIC magnification maps and then alternatively recover the LFs with the CATS, GRALE, Zitrin-LTM, and median parametric magnification maps.

The result is shown in Figure 15, and excellent recovery of the LF is observed brightward of -16.5 mag for all magnification maps. The best performance is achieved using the median magnification map; however, we note that faintward of -15 mag, the recovered LF still diverges from the input LF, rapidly transitioning faintward of -15 to a faint-end slope of -2 .

D. ESTIMATES OF THE FAINT-END SLOPES IN PREVIOUS WORK USING ONLY THE HFF DATA

In utilizing the data from the HFF clusters to map out the faint-end of the UV LF and derive faint-end slope results, it is valuable to perform this exercise using only the HFF samples to preserve the independence of the faint-end slope determinations from those derived from the field (i.e., the HUDF). By doing so, one can conduct fair comparisons between faint-end slope results α derived using lensing clusters and from the field to test for consistency.

Towards this end, we have taken the binned LF results from L16 on the HFF clusters and fit the results to a power law to estimate a faint-end slope α . The results are presented in Figure 16 as the solid lines and give slopes of -2.15 ± 0.09 , -2.39 ± 0.24 , and -1.98 ± 0.27 at $z \sim 6$, $z \sim 7$, and $z \sim 8$, respectively. Interestingly, these results are mostly steeper than the faint-end slopes inferred from field searches at the relevant redshifts. Part of this difference could be due to the modest bias towards steeper slopes as a result of the large sizes L16 use in estimating the selection volumes (Bouwens et al. 2016: see their Figure 2).

We can obtain even stronger constraints on the faint-end slope α results from the HFF clusters by having at least one point on the bright end of the LF from field searches to use as an anchor. There is not much search volume available behind clusters to constrain this part of the LF, and so including this information is useful. We therefore refit the $z \sim 6$, $z \sim 7$, and $z \sim 8$ LF results on the HFF clusters from L16, anchoring the fit results to the field LF results from the same group, i.e., Finkelstein et al. (2015), at -20 mag using their best-fit Schechter function. We chose -20 mag somewhat arbitrarily to be close enough to the knee of the LF, i.e., ~ -21 mag, while not being so bright as to be affected by uncertainties in the assumed characteristic luminosity or form of the bright end of the LF (Schechter vs. power-law: i.e., Bowler et al. 2015).

The fits are presented in Figure 16 as the dotted lines. The faint-end slopes in this case are -2.23 ± 0.05 , -2.19 ± 0.08 , and -2.06 ± 0.15 for the $z \sim 6$, $z \sim 7$, and $z \sim 8$ LFs, respectively. These values are consistent with the faint-end slope α results we derive from the HFF results from L16 without a bright anchor point.